https://doi.org/10.5194/acp-2020-1285
Preprint. Discussion started: 5 January 2021

Atmospheric Chemistry and Physics Discussions

New particle formation inside ice clouds: In-situ observations in the tropical tropopause layer of the 2017 Asian Monsoon Anticyclone

Ralf Weigel[1], Christoph Mahnke[2,6], Manuel Baumgartner[1,3], Martina Krämer[1,4], Peter Spichtinger[1], Nicole Spelten[4], Armin Afchine[4], Christian Rolf[4], Silvia Viciani[5], Francesco D'Amato[5], Holger Tost[1], and Stephan Borrmann[1,2]

[1]Institut für Physik der Atmosphäre, Johannes Gutenberg Universität, Mainz, Germany
[2]Partikelchemie, Max-Planck-Institut für Chemie, Mainz, Germany
[3]Zentrum für Datenverarbeitung, Johannes Gutenberg University, Mainz, Germany
[4]Institute of Energy and Climate Research (IEK-7), Forschungszentrum Jülich, Jülich, Germany
[5]National Institute of Optics - National Research Council (CNR-INO), Florence, Italy
[6]now at the Institute of Energy and Climate Research (IEK-8), Forschungszentrum Jülich, Jülich, Germany

Abstract

From 27 July to 10 August 2017 the airborne StratoClim mission took place in Kathmandu, Nepal where eight mission flights were conducted with the M-55 *Geophysica* up to altitudes of 20 km. New Particle Formation (NPF) was identified by the abundant presence of ultrafine aerosols, with particle diameters d_p smaller than 15 nm, which were *in-situ* detected by means of condensation nuclei counting techniques. NPF fields in clear-skies as well as in the presence of cloud ice particles ($d_p > 3$ µm) were encountered at upper troposphere / lowermost stratosphere (UT/LS) levels and within the Asian Monsoon Anticyclone (AMA). NPF-generated ultrafine particles in elevated concentrations (N_{uf}) were frequently found together with cloud ice (in number concentrations N_{ice} of up to 3 cm^{-3}) at heights between ~ 11 km and 16 km. From a total measurement time of ~ 22.5 hours above 10 km altitude, in-cloud NPF was in sum detected over ~ 1.3 hours (~ 50 % of all NPF records throughout StratoClim). Maximum N_{uf} of up to ~ 11000 cm^{-3} were detected coincidently with intermediate ice particle concentrations N_{ice} of 0.05 – 0.1 cm^{-3} at comparatively moderate carbon monoxide (CO) contents of ~ 90 - 100 nmol mol^{-1}. Neither under clear-sky nor during in-cloud NPF do the highest N_{uf} concentrations correlate with the highest CO mixing ratios, suggesting that an elevated pollutant load is not a prerequisite for NPF. Under clear-air conditions, NPF with elevated N_{uf} (> 8000 cm^{-3}) occurred slightly less often than within clouds. In the presence of cloud ice, NPF with N_{uf} between 1500 – 4000 cm^{-3} were observed about twice as often as under clear air conditions. When ice water contents exceeded 1000 µmol mol^{-1} in very cold air (< 195 K) at tropopause levels NPF was not found. This may indicate a reduction of NPF once a strong overshoot is prevalent together with the presence of mainly *liquid-origin* ice particles. In the presence of *in-situ* cirrus near the cold point tropopause very recent NPF or events of remarkable strength (mixing ratios $n_{uf} > 5000$ mg^{-1}) were rarely observed (~ 6 % of in-cloud NPF data). For specifying the constraining mechanisms for NPF possibly imposed by the microphysical

https://doi.org/10.5194/acp-2020-1285
Preprint. Discussion started: 5 January 2021

Atmospheric Chemistry and Physics Discussions

properties of the cloud elements, the integral radius (*IR*) of the ice cloud population was identified as the most practicable indicator. Neither of both, the number of ice particles or the free distance between the ice particles, is clearly related to the NPF-rate detected. The results of a numerical simulation indicates how the *IR* affects the supersaturation of a condensable vapour, such as sulphuric acid, and that *IR* determines the effective limitation of NPF rates due to cloud ice.

1. Introduction

The process of gas-to-particle conversion, also denoted as homogeneous aerosol nucleation and most commonly known as new particle formation (NPF), constitutes one of the most effective sources of atmospheric aerosols and cloud condensation nuclei, which could promote the cloud formation at intermediate and upper tropospheric altitudes (e.g. Spracklen et al. (2006); Merikanto et al. (2009); Dunne et al. (2016); Gordon et al. (2017)). Sulphuric acid (H_2SO_4) and water (H_2O) presumably are important chemical compounds involved in the NPF process which, moreover, is likely aided when ions come into play at elevated altitudes and cold temperatures within the atmosphere (Lee et al. (2003); Kazil et al. (2008); Weigel et al. (2011); Duplissy et al. (2016)). It was suggested that a ternary nucleation process involves, apart from sulphuric acid and water, an additional constituent such as ammonia (NH_3; Ball et al. (1999); Benson et al. (2009); Höpfner et al. (2019)). Experimental studies at the CLOUD (Cosmics Leaving OUtdoor Droplets) chamber confirmed that NPF rates are substantially elevated within this ternary H_2SO_4-H_2O-NH_3 System (e.g. Kirkby et al. (2011); Kürten et al. (2016); Kürten (2019)).

From the CLOUD experiments, which were performed under a variety of controlled conditions, it can be deduced that the intensity of NPF (the formation rate of new particles per air volume and per time unit) depends on the concentration of the NPF precursors. The results of individual experiments (Kürten et al. (2015); Kürten et al. (2016)) at different and elevated concentrations of the H_2SO_4 solution, always at supersaturated states, show that the nucleation rates are strongly associated with the precursor concentrations. Temperature determines the degree of supersaturation, which implies that even high precursor concentrations may result in a weak NPF rate, and vice versa. In particular, for ternary or multi-component NPF, the degree of supersaturation as a function of temperature remains indeterminable. Therefore, the chamber experiments allow for studying the nucleation rate as a function of the precursor concentration at different temperatures, i.e. at supersaturation ratios, which are specific, but mostly unknown, with respect to the system of nucleating substances (involving H_2SO_4, H_2O, and NH_3). The complexity increases with sulphuric acid nucleation systems involving besides NH_3 also nitric acid (HNO_3) (Wang et al., 2020) or oxidised organic vapours (Riccobono et al., 2014), all of which may promote the NPF process at supersaturations lower than required for pure H_2SO_4 solutions.

https://doi.org/10.5194/acp-2020-1285
Preprint. Discussion started: 5 January 2021


Atmospheric Chemistry and Physics Discussions

The role of organic substances in connection with NPF could be of particular importance in the tropical UT/LS as has been indicated by (Schulz et al., 2018) and (Andreae et al., 2018). The time series of a nucleation event within the CLOUD chamber (supplementary material of Kirkby et al. (2011)) shows, however, that the nucleation rate remains elevated as long as the amount of precursors is kept at a constant level as investigated by means of the CLOUD experiments. Under real conditions in the atmosphere, however, the concentration of precursor material is spatially and temporally highly variable. Temperature fluctuations affect the degree of precursor supersaturation; hence, even low precursor concentrations may result in elevated supersaturations and intense NPF. The influence of third or multiple substances possibly involved in the NPF process is not unambiguously detectable or even quantifiable in the ultrafine particle population due to the current lack of instrumentation capable of analysing the chemical composition of such small particles directly.

By means of ground based as well as airborne *in-situ* measurements, NPF was frequently observed to occur at various conditions and atmospheric altitudes (Kerminen et al., 2018). Recently, Williamson et al. (2019) compiled a comprehensive data set of *in-situ* NPF observations at altitudes from 180 m above sea level to up to ~ 12 km, thereby covering a latitude range from 80° North to 70° South alongside the Americas, and by probing air over both oceans, the Pacific and the Atlantic. In tropical regions, most of the *in-situ* NPF observations were made below the level of zero net radiative heating, i.e. at altitudes where subsidence or cloud formation is still well capable to efficiently remove or scavenge aerosol particles.

Investigations concerning the occurrence of NPF within clouds, or in their immediate vicinity, are sparse and are mainly limited to tropospheric altitudes. The region above tropospheric clouds seems favourable for NPF to occur, and possible reasons for this are discussed by Wehner et al. (2015). Furthermore, NPF was found to be an important process inside the convective outflows (e.g. Twohy et al. (2002); Waddicor et al. (2012)). From measurements in the upper troposphere it is commonly assumed that the occurrence of NPF is directly connected to deep convective cloud systems (e.g. de Reus et al. (2001); Clarke and Kapustin (2002); Weigelt et al. (2009); Andreae et al. (2018)). The relationship between NPF and ice clouds is discussed in this study, whilst the immediate connection of NPF and deep convective events is addressed in Weigel et al. (2020a).

During *in-situ* measurements aboard the NASA high altitude research aircraft WB-57, Lee et al. (2004) observed nucleation events inside subtropical and tropical cirrus clouds between 7 and 16 km over Florida. The same authors summarise that they found recent occurrence of NPF in 72 % of their measurements within clouds. Despite the conceptual notion that the presence of cloud elements generally inhibits the formation of new particles, Kazil et al. (2007)

https://doi.org/10.5194/acp-2020-1285
Preprint. Discussion started: 5 January 2021


Atmospheric Chemistry and Physics Discussions

demonstrated by means of model simulations that new sulphate aerosol can form within ice clouds such as cirrus. New particles are also produced in the anvil region and cirrus decks of Mesoscale Convective Systems (MCS) over West Africa (Frey et al., 2011). The particular role of mid-latitude MCS as a source of freshly formed aerosol within the upper troposphere was already suggested by Twohy et al. (2002), based on the detection of increased concentrations of particles with size diameter (d_p) greater than 25 nm, concurrently with elevated particle volatility. In the region of the Tropical Transition Layer (TTL) over South America, Australia and West Africa, the *in-situ* measurements by Weigel et al. (2011) revealed nucleation mode particles in elevated number concentrations likely resulting from recent NPF. Based on coincident detections of abundant nucleation mode particles together with cloud elements (i.e. ice particles of diameters 2.7 µm < d_p < 1.6 mm) in ice number concentrations always below ~ 2 cm^{-3} the authors concluded that the occurrence of NPF is mainly limited by the number of cloud particles. The underlying concept is that the surfaces of the cloud elements either scavenge the NPF-produced aerosol particles or remove the nucleating vapour molecules prior to the NPF process.

Regarding the occurrence of NPF in conjunction with the presence of upper tropospheric ice clouds, still several unspecified details remain:

1) what are the sets of chemical species acting as NPF precursor,
2) does NPF possibly require (or not) contributions by cosmic radiation, ions (Lovejoy et al. (2004); Kazil et al. (2008); Weigel et al. (2011)) or chemical agents or catalysts (e.g. Kürten (2019)),
3) which are the advantageous thermodynamic conditions for NPF within a cloud, and
4) the conditions under which NPF is suppressed by the presence of ice particles of certain size and/or number.

Comprehensive understanding of these processes and their influences under real atmospheric conditions potentially contributes to narrow down the cloud type and the in-cloud location where NPF preferentially occurs, in order to obtain estimates (in particular for modelling purposes) concerning the importance of in-cloud NPF. Furthermore, the question could arise how the ultrafine particles generated by in-cloud NPF are processed: for example, if the ultrafine particles disperse as contribution to the clear air background aerosol as soon as the cloud elements evaporate, or if, in persistent clouds, the ultrafine particles are captured by present ice particles. In the context of the Asian Monsoon Anticyclone (AMA) it is important to clarify the origin of observed enhancements of aerosols in the embedded Asian Tropopause Aerosol Layer (ATAL, cf. Vernier et al. (2011); Vernier et al. (2018)). NPF could well be an important source of aerosol particles which are then available for further processing to form the ATAL (Höpfner et

https://doi.org/10.5194/acp-2020-1285
Preprint. Discussion started: 5 January 2021


Atmospheric Chemistry and Physics Discussions

al. (2019); He et al. (2019); Mahnke et al. (2020)). Furthermore, the relative contribution of in-cloud versus clear-air NPF is of importance in this context.

The Asian Monsoon Anticyclone (AMA) constitutes one of the most important weather systems, which mainly determines the circulation in the Upper Troposphere/Lower Stratosphere (UT/LS) during monsoon season over the Indian subcontinent. The AMA is usually associated with extensive deep convection capable of transporting polluted air from the regional boundary layer (BL) to high altitudes. From the beginning of June through about the end of September, the large-scale anticyclone persists in the altitude level from the UT reaching up into LS regions (e.g. Randel and Park (2006); Park et al. (2007)) spanning over longitudes from East Asia to the Middle East/East Africa (e.g. Vogel et al. (2014); Vogel et al. (2019)). The system's anticyclonic rotation induces the development of a horizontal transport barrier within in the UT/LS (Ploeger et al., 2015) reducing isentropic exchange between the interior of the AMA and the anticyclone's surroundings. The vertical upward transport within the Asian monsoon circulation is understood as an effective pathway for young air of BL - origin (Vogel et al., 2019) to rapidly reach UT/LS altitudes, accompanied by various constituents such as pollutants and further gaseous material (Pan et al., 2016) and in particular water vapour (Ploeger et al., 2013). To which extent the stratospheric entry of H_2O is supported by cirrus cloud particles (as a result of overshooting convection or ice formation due to local dynamics; de Reus et al. (2009); Corti et al. (2008)) is currently under debate (Ueyama et al. (2018), and references therein) and one of the subjects of a recent study by Krämer et al. (2020). Based on satellite investigations the existence of the ATAL was explored at tropopause altitudes within the AMA region (Vernier et al. (2011); Thomason and Vernier (2013)). Therefore, the constituents of the uplifted young air from low altitudes may also comprise the precursor material from anthropogenic (Vernier et al. (2015); Yu et al. (2015); Höpfner et al. (2019); Mahnke et al. (2020)) and other sources to develop and maintain the observed aerosol layer, most likely due to NPF occurring at levels between approximately 14 km and the tropopause.

This study reports on the frequent occurrence of NPF in the presence of cloud ice in the tropopause region over the Indian subcontinent during the Asian monsoon season. All measurement data shown herein were acquired during StratoClim 2017 (in July/August 2017) based at Kathmandu, Nepal, and conducted with the M-55 *Geophysica* that operates up to 20 km altitude. NPF was observed with almost equivalent extent in clear-air as well as, under certain conditions, in the midst of cloud ice particles. This investigation aims at summarising the various conditions under which NPF was observed coincidently with cloud ice particles. Close examination of the measured data revealed that potential artefacts on the aerosol measurements due to the presence of ice particles, as suggested by Williamson et al. (2019), are

https://doi.org/10.5194/acp-2020-1285
Preprint. Discussion started: 5 January 2021


Atmospheric Chemistry and Physics Discussions

largely excludable for the StratoClim data set (cf. Appendix A). The caveats limiting the magnitude of encountered NPF are examined, as are the possibly constraining mechanisms imposed by the cloud elements' microphysical properties. The frequency of NPF observation in coincidence with elevated ice particle densities puts emphasis on the importance of the tropopause region within the AMA as an effective source region of freshly nucleated aerosol.

2 The StratoClim field campaign in 2017, instruments and methods

During the Asian monsoon season, between 27 July and 10 August 2017, a total of eight scientific flights was conducted above parts of the Indian subcontinent, out of Kathmandu, Nepal (27° 42' 3'' N, 85° 21' 42'' E) throughout StratoClim 2017 (cf. Figure 1). Some of these flights partly led out of the Nepalese airspace, to east India, Bangladesh and the farthest north of the Bay of Bengal. The occurrence of NPF was encountered (cf. Figure 1) during each flight, either in clear air or in the presence of cloud (ice) particles.

2.1 Number concentration of sub-micrometre sized particles

The 4-channel continuous flow condensation particle counter COPAS (COndensation PArticle counting System; Weigel et al. (2009)), which was operated with the chlorofluorocarbon (FC 43) as working liquid, was used for measuring aerosol particle number concentrations. Particle detection and data storage occurred at 1-Hz frequency. For the reduction of the statistical noise in the raw signals, which are recorded directly from the scattered light detectors of the COPAS instrument, the 1-Hz raw data are pre-processed by a 15-second running average. The COPAS channels were set to different 50 %-detection particle diameters d_{p50} (i.e. 6 nm, 10 nm, and 15 nm). By counting aerosols (with d_{p50} = 10 nm) downstream of a heated (~ 270°C) sample flow line, a fourth COPAS channel measured particle concentrations of non-volatile (nv) or refractory particles (e.g. soot, mineral dust, metallic aerosol material as well as, e.g., organic material mixtures not evaporating at 270 °C, etc.). By means of laboratory experiments, the aerosol heating device was demonstrated to vaporise more than 98 % of H_2SO_4-H_2O particles at pressures between 70 and 300 hPa (Weigel et al., 2009). The aerosol sampling occurred via the forward facing aerosol inlet of COPAS, a custom-made reproduction of the inlet used on board the NASA ER-2 (Wilson et al., 1992). The use of this aerosol inlet also facilitated Lee et al. (2004) to measure in-cloud NPF. The inlet allows for aerosol sampling well outside the boundary layer of the aircraft. The inlet's geometry comprises two serial diffusors to sample air (at super-isokinetic conditions) with decelerated flow speed compared to the ambient free flow. The largest particle diameter that is detectable with the COPAS system is confined by the inlet geometry, and it is estimated that sub-micrometre sized particles enter the aerosol inlet and pass the aerosol lines without significant particle losses (Weigel et al., 2009). However, aerosol particles with diameter of up to 5 µm may occasionally be aspired by the COPAS inlet, but are

https://doi.org/10.5194/acp-2020-1285
Preprint. Discussion started: 5 January 2021


Atmospheric Chemistry and Physics Discussions

clearly undersampled (Ebert et al., 2016). The COPAS measurement uncertainty is about 15 % for stratospheric particle concentrations, mainly due to uncertainties in the volume flow and as a result from particle counting statistics. The COPAS is an established instrument for high altitude application, its performance was characterised by Weigel et al. (2009) and COPAS data were used and discussed in various studies (e.g. in Curtius et al. (2005); Borrmann et al. (2010); Frey et al. (2011); Weigel et al. (2011); Weigel et al. (2014); Schumann et al. (2017); Höpfner et al. (2019)).

2.2 Terminology and notations

The measured particle number concentrations N are provided in units of particle number per cubic centimetre of sampled air (ambient conditions). To compare aerosol observations from different pressure altitudes and, e.g., for correlations with mixing ratios of trace gases, COPAS measurements are also given as mixing ratio n in units of particles per milligram of air (mg^{-1}) as calculated based on the 1-Hz-resolved data of ambient static pressure and temperature (cf. Section 3.5). Hereafter, n_{10} denotes the mixing ratio of particles with diameters larger than 10 nm. The detection of the particle number concentration or mixing ratio at different d_{p50} (i.e. N_6 or n_6 for particles with $d_p > 6$ nm, and N_{15} or n_{15} for $d_p > 15$ nm), aims at the identification of recent new particle formation, principally based on the difference of both quantities (cf. Weigel et al. (2011)). The number concentration of ultrafine aerosol particles (hereafter denoted as N_{uf}) is calculated from the difference N_6 - N_{15} = $N_{6\text{-}15}$ and serves as an indication for recent NPF if the designated NPF criterion is met:

$$0.8 \cdot N_6 - 1.2 \cdot N_{15} > 0 \qquad (1),$$

based on the principle definition used by Weigel et al. (2011). Further details concerning the corrections applied to the measured COPAS data, which were obtained throughout StratoClim 2017, are provided by Weigel et al (2020a), where the empirical parameters of 0.8 and 1.2 are introduced.

If compliant with the NPF criterion, a series of data points is a designated event if measured number concentrations (or mixing ratios) of ultrafine particles continuously remain greater than zero over at least five consecutive seconds. Caveats with this event definition are inherent for observations as short as 1 – 5 seconds. Due to the detector's signal-to-noise-ratio and counting statistics, the given quantity and durations of too short events bear significant uncertainties. In addition, however, this event definition may prevent resolving very fine spatial structures (i.e. horizontally on 150 m-scales, vertically on 10 m-scales) of NPF fields. With the mean airspeed of the M-55 *Geophysica* (~ 154 ± 39 m s^{-1}), the event definition implies that within five seconds a horizontal distance of ~ 770 m (in flight direction) is covered. The total of 308 individual

https://doi.org/10.5194/acp-2020-1285
Preprint. Discussion started: 5 January 2021

Atmospheric Chemistry and Physics Discussions

detections of elevated N_{uf} coincidently with the presence of cloud elements, 104 of which fulfilled the event criterion. Note that the in-cloud NPF events discussed herein are partially embedded in a larger NPF fields, which are identified by successive, uninterrupted detections of elevated N_{uf}. Within this larger NPF fields the duration of simultaneous ice particles detection could be shorter or interrupted. One or more in-cloud NPF events could be subsets of NPF events with continuously elevated N_{uf} concentration, which are generally discussed by Weigel et al. (2020a). They (*ibid.*) also present further details concerning the duration of NPF events, the persistence of the freshly formed particles in the ultrafine size range, and the presence of non-volatile particles under NPF conditions during StratoClim 2017.

The NPF-rate and, hence, the intensity of NPF varies with the degree of supersaturation of the NPF precursor (Kirkby et al. (2011), Kürten et al. (2016)). Hereafter, the strength of a NPF event is classified as

(1) *excessive* NPF if detected aerosol densities of ultrafine particles exceed
   - mixing ratios of 10000 mg^{-1} or
   - number concentrations of 5000 cm^{-3},

(2) *intermediate* NPF when number densities of ultrafine particles range at
   - mixing ratios of 1000 $mg^{-1} < n_{uf} < 10000$ mg^{-1} or
   - number concentrations of 500 $cm^{-3} < N_{uf} < 5000$ cm^{-3}, and

(3) *weak* NPF when
   - mixing ratios n_{uf} remain below 1000 mg^{-1}, or
   - number concentrations N_{uf} of less than 500 cm^{-3} are detected.

(4) The notation *most intense* NPF is often used synonymously with *most recent* NPF in the following.

As the persistence of the particles in the ultrafine size range is short (i.e. a few hours only, cf. Weigel et al. 2020a), an intense NPF event could still be in process when observed, or it had been completed very recently, i.e. 1-2 hours prior to the detection. However, for a NPF encounter with low or intermediate number densities of ultrafine particles (n_{uf} or N_{uf}), the conclusions concerning the event's age remain ambiguous, as it can be caused by weakly proceeding NPF or by NPF, which had occurred several hours ago.

2.3 Cloud particle and water vapour detection

The NIXE-CAPS (New Ice eXpEriment: Cloud and Aerosol Particle Spectrometer, in the following denoted as NIXE) was deployed during StratoClim for measuring the number size distribution in the cloud particles' diameter size range of 3 – 930 µm with 1-Hz resolution (Luebke et al. (2016); Costa et al. (2017)). Comprehensive numerical analyses by means of computations fluid

https://doi.org/10.5194/acp-2020-1285
Preprint. Discussion started: 5 January 2021

Atmospheric Chemistry and Physics Discussions

dynamics (CFD) were carried out by Afchine et al. (2018) to investigate the impact of the instrument's position underneath the aircraft wing on the cloud particle detection. The NIXE-CAPS consist of two detectors: the NIXE-CAS-DPOL (Cloud and Aerosol Spectrometer with Detection of POLarization) and the NIXE-CIPg (Cloud Imaging Probe – grayscale). Compiling measured data of both independent detectors delivers microphysical properties, in terms of size and number, of particles with diameters ranging from 0.61 µm to 937 µm. The methods of post flight data processing and corrections were described by Luebke et al. (2016). Cloud particle detections were recognised as such when particles of diameters > 3 µm were encountered in numbers greater than zero. Hereafter, the number concentration of ice particles is denoted as N_{ice} (i.e. $N_{3\text{-}937\mu m}$, the number concentration of ice particles with diameters of 3 µm < d_p < 937 µm). The data of ice water content (*IWC*) used herein were ascertained by using the relationship of cloud particles' mass (m_p) to diameter (d_p) (Krämer et al. (2016); Luebke et al. (2016); Afchine et al. (2018)).

The closed-path Lyman-α photo-fragment fluorescence hygrometer FISH (Fast In situ Stratospheric Hygrometer; cf. Zöger et al. (1999) and Meyer et al. (2015)) allows for 1-Hz resolved measurements of the atmosphere's gaseous and solid phase water, denoted as total water or H_2O_{tot}. The FISH detection of H_2O_{tot} covers mixing ratios of 1 - 1000 µmol mol^{-1} over atmospheric pressures ranging from 50 hPa to 500 hPa with an accuracy and precision of 6 – 8 % and 0.3 µmol mol^{-1}. The ice water content (*IWC*) was calculated by subtracting the H_2O_{Gas} (measured by another Lyman-α detector, FLASH, the FLuorescent Airborne Stratospheric Hygrometer) from H_2O_{tot}. For further detail concerning the data processing, see Afchine et al. (2018). Dependent on ambient temperatures, the smallest *IWC* detectable by the FISH instrument is about $1 \cdot 10^{-3}$ µmol mol^{-1} and $20 \cdot 10^{-3}$ µmol mol^{-1}, which corresponds to approximately $1 – 20 \cdot 10^{-4}$ mg m^{-3} (Afchine et al., 2018).

To cover the wide range of *IWC* observed during the StratoClim mission (from thousandths to thousands of µmol mol^{-1}) the complementary data sets of NIXE-CAPS and FISH concerning *IWC* were merged. Thus, when large ice particles were abundant, causing *IWC* of hundreds to thousands of µmol mol^{-1}, mostly NIXE-CAPS data contributed to the resulting *IWC* data. In contrast, low numbers of small ice particles caused the FISH instrument to provide the most reliable *IWC*. The overall uncertainty of given *IWC* values were estimated to be ~ 20 % (Krämer et al., 2020).

Based on cloud particle (NIXE-CAPS) and water vapour (FISH) measurements, ice particle shattering, which could be indicated e.g. by short bursts of small ice particles, remained unobserved throughout StratoClim (Krämer et al., 2020).

https://doi.org/10.5194/acp-2020-1285
Preprint. Discussion started: 5 January 2021

Atmospheric Chemistry and Physics Discussions

2.4 Carbon monoxide

In the troposphere, carbon monoxide (CO) is a component of atmospheric pollution (Park et al., 2009), the main sources of which are both natural and anthropogenic (including combustion, and the oxidation of hydrocarbons). It is assumed that the contributions to the tropospheric CO budget almost equivalently originate from: (1) its photochemical production and (2) directly from sources located at the surface. Mainly the oxidation with hydroxyl radical (OH) depletes CO within the atmosphere (Logan et al. (1981); Yin et al. (2015)). CO mixing ratios are well suitable and often used as tropospheric tracer for air's transport (a) within the troposphere, (b) across the tropopause, and (c) within the lower stratosphere. In the free troposphere, CO mixing ratios range from unpolluted 50 nmol mol^{-1} up to mixing ratios well exceeding 700 nmol mol^{-1} in close vicinity to emission sources (Clerbaux et al. (2008), Park et al. (2009)). Inside the AMA and up to 15 km altitude, CO mixing ratios remain comparatively high ($\gtrsim$ 100 nmol mol^{-1}), while between 15 km and 20 km altitude the CO mixing ratios decrease monotonically down to $\sim$ 40 nmol mol^{-1} (Park et al., 2009).

During the StratoClim mission, the mixing ratio of CO was measured by means of the Tunable Diode Laser (TDL) technique implied in the revised version of the Cryogenically Operated Laser Diode (COLD) spectrometer. Compared to the previous instrument version (4 s temporal resolution, Viciani et al. (2008)), COLD-2 integrates improvements (Viciani et al., 2018) regarding:

1) an increased measurement's resolution by a factor of four,
2) an enhanced in-flight sensitivity of the COLD-2 spectrometer (ranging at $\sim$ 2 nmol mol^{-1} at integration times of 1 s) , and
3) an accuracy of 3 % is specified for the CO measurement with COLD-2.

Within the data set of simultaneous measurements with COPAS, COLD-2 detected minimum and maximum CO mixing ratios of 14 nmol mol^{-1} and 153 nmol mol^{-1}, respectively.

2.5 Data of ambient temperature and static pressure

The atmospheric temperature and pressure data were taken from the Unit for Connection with the Scientific Equipment (UCSE, Sokolov and Lepuchov (1998)), a part of the navigational system of the M-55 *Geophysica*. UCSE data are provided as 1-Hz-resolved ambient pressure (with an accuracy of ±1 hPa) and temperature (±2 K accuracy).

The potential temperature θ is calculated correspondingly with 1-Hz resolution in compliance with the definition by the World Meteorological Organization (WMO, 1966). Note that for the given vertical temperature gradients and over the θ -range covered during StratoClim 2017 (i.e.

https://doi.org/10.5194/acp-2020-1285
Preprint. Discussion started: 5 January 2021


Atmospheric Chemistry and Physics Discussions

348 up to ~ 477 K), the WMO recommended calculation of θ differs only by up to ~ 1 K from the
349 values obtained by using the recently reappraised θ-calculation (Baumgartner et al., 2020).

350 3 Observations and results

351 During StratoClim 2017, eight mission flights were conducted with a total of 36.6 hours, whereas
352 over a total of 6.42 hours ice clouds were encountered at air temperatures colder than 240 K.
353 The cirrus cloud observations are described and comprehensively discussed by Krämer et al.
354 (2020), and thus are only briefly summarised herein. Most of the in-cloud measurements during
355 StratoClim 2017 were performed at temperatures $\lesssim$ 205 K, corresponding to potential
356 temperatures above ~ 355 K and altitudes higher than ~ 14 km, i.e. well within the TTL region.
357 The clouds observed during the Asian monsoon season include: 1) *in-situ* cirrus, which had
358 formed in calm dynamic situations associated with very slow updraught as well as 2) *liquid-*
359 *origin* cirrus, the formation of which is connected to overshooting deep convection with elevated
360 uplift velocities (see Section 5.2), including ice clouds (e.g. anvils) associated with convective
361 outflow.

362 At temperatures colder than 205 K, N_{ice} and *IWC* often reached values above their respective
363 median of 0.031 cm^{-3} (blue dashed line in Figure 2) and ~ 0.2 – 2 µmol mol^{-1} (cf. Figure 6). The
364 highest observed values at these temperatures are reached with *IWC* of up to 1000 µmol mol^{-1}
365 and a maximum N_{ice} as high as 30 cm^{-3}. Moreover, the ice crystals sizes (not shown here) exceed
366 their corresponding median, hence, comparatively large ice crystals were found up to and
367 around the cold point tropopause. Such large particles were detected during flights in strong
368 convection.

369 3.1 The distribution of NPF and the presence of cloud ice particles over day time

370 During a total of ~ 22.5 hours of COPAS measurement time at altitudes above 10 km ($\theta \gtrsim$ 350 K),
371 in general, a duration of about 2 hours and 38 minutes was spent under NPF conditions in the
372 TTL region (~ 11-17.5 km, ~ 355 – 400 K, cf. Weigel et al 2020a). Throughout the entire
373 StratoClim mission, elevated number densities of ultrafine particles were observed coincidently
374 with cloud particles (N_{ice} > 0 cm^{-3}) over a total of about 1 hour and 17 minutes (cf. Table 1). The
375 encountered in-cloud NPF events at altitudes between approximately 11 km and 16.5 km
376 (~ 355 – 385 K) had a mean event duration of 14.5 seconds (ranging from one second to a
377 maximum of about 300 seconds).

378 In Figure 2, all NPF detections throughout the StratoClim mission are compiled within a 1-day
379 time series to illustrate the diurnal variability of the observations. The scale of the time series is
380 limited to the daytime as the eight mission flights were conducted between 03:30 (UTC) and
381 12:30 (UTC), which corresponds to local times of 09:15 LT to 18:15 LT. Kathmandu local noon

https://doi.org/10.5194/acp-2020-1285
Preprint. Discussion started: 5 January 2021


Atmospheric Chemistry and Physics Discussions

time corresponds to 22500 seconds of day, or 06:15 UTC, and is tagged with an orange line in Figure 2. The encounter of NPF is considered as clear-air observation (black data points in Figure 2, complete StratoClim data set) when simultaneously detected cloud (ice) particle number concentration N_{ice} remained at 0 cm^{-3}. Coincident observations of NPF and cloud (ice) particles (N_{ice} > 0 cm^{-3}) are highlighted by red data points in Figure 2. The increased frequency of abundant cloud ice in the local afternoon may temporally coincide with the typically elevated convective activity during the second half of a day. However, a temporal dependency was not observed for the occurrence, the strength or the frequency of NPF. Furthermore, there is no obvious indication that the number of ice particles present had a direct influence on the NPF strength. The impression arises that even intense NPF happens almost unaffected only by the number of present cloud ice particles, as otherwise likely larger differences should be visible between the N_{uf} maxima in clear air and under in-cloud conditions.

3.2 Vertical distribution of ultrafine particles in presence/absence of cloud ice particles

Figure 3 displays the vertical distribution of NPF-generated ultrafine aerosols in terms of the mixing ratio n_{uf} as a function of potential temperature. The panel a) of Figure 3 depicts the clear-air observations of elevated n_{uf} (black) together with those when coincidently ice particles were detected (red). The coincident observation of ice particles and ultrafine aerosol is vertically limited to a range of potential temperatures from 355 K to 385 K (cf. also Table 1). Recent convective overshooting to altitudes above the mean tropopause height (~ 380 K, averaged over the period and operation area of StratoClim 2017) is indicated by θ values significantly larger than 380 K. Clear-air NPF was sampled also at higher altitudes, i.e. at potential temperatures above 385 K and up to ~ 400 K, or at lower altitudes, below 355 K. As indicated by the time series shown in Figure 2, also the vertical profiles suggest that the strength of NPF was largely independent from the presence of cloud elements. The data in Figure 3b show that in-cloud NPF observations were made during each of the eight mission flights (cf. Figure 1). Apparently, in-cloud NPF is a common phenomenon in connection with the AMA and in presence of prevailing large convective cloud systems over the Himalayan foothills. The separation of in-cloud and clear-air conditions of NPF observation is illustrated with the intermediate panels (c and d) of Figure 3. In this way, the in-cloud NPF observations (c), which occurred in the altitude interval of ~ 355 < Θ < 385 K, are opposed to NPF observations that were exclusively made under clear-air conditions (d) over a vertical range between 355 K and 400 K.

The relationship between CO mixing ratios and NPF occurrence in the tropical UT/LS over West-Africa (Weigel et al., 2011) indicated a relationship between NPF and ground sources of gaseous NPF precursor substances (mainly sulphur compounds, potentially also organics) that are

https://doi.org/10.5194/acp-2020-1285
Preprint. Discussion started: 5 January 2021


Atmospheric Chemistry and Physics Discussions

417 efficiently lifted into the TTL region via convective transport, and not entirely removed by
418 scavenging. Tost et al. (2010) revealed a substantial underestimation of simulated SO_2 compared
419 to flight observations throughout the SCOUT-O3 mission in 2005. These authors utilised global
420 chemistry climate model simulations independent of the representation of deep convection, the
421 results of which indicated that the scavenging of SO_2 is weaker than expected and that the
422 impact of retention is not negligible (*ibid.*). However, a substantial fraction of the well soluble
423 sulphur dioxide (SO_2) may not reach UT/LS altitudes via convective events. Cloud-resolving
424 numerical modelling revealed a fraction of 40-90 % of SO_2, that is capable of reaching the deep
425 convection's outflow region (Barth et al., 2001), largely consistent with the estimates by Crutzen
426 and Lawrence (2000). The results of other model studies (Ekman et al., 2006) showed that only
427 30 % of SO_2 from the boundary layer reach cloud top levels. Experimental studies by Jost et al.
428 (2017) found moderate retention coefficients (0.2 – 0.5) of SO_2 in the ice phase of clouds, while
429 hydrochloric acid (HCl) and nitric acid (HNO_3) are entirely retained under ice cloud conditions
430 (*ibid.*). Once the cloud particles freeze, large fractions of the in-cloud dissolved SO_2 could leave
431 the cloud-ice composite. The SO_2 remaining in the cloud ice composite, is released as soon as the
432 ice sublimates in the region of convective outflow, or underneath, while the ice particles
433 sediment.

434 NPF should most frequently occur in air enriched with precursor material and which
435 experienced rapid vertical uplift. An indicator for the air masses' pollutant load and/or contact
436 with the boundary layer and recent vertical uplift is provided by air's carbon monoxide (CO)
437 content. According to the CO mixing ratio when n_{uf} mixing ratios were elevated (colour coding in
438 panels e and f of Figure 3), none of the different NPF conditions, in clear air or in the presence of
439 ice particles, shows the highest number of ultrafine particles together with highest CO mixing
440 ratio. In fact, the highest densities of ultrafine particles were observed at comparatively
441 moderate CO mixing ratios of ~ 90 - 100 nmol mol^{-1}. This largely agrees with the in-situ
442 measurements of correlations between CO mixing ratio and NPF obtained at similar altitudes in
443 the region of Mesoscale Convective Systems during the West African Monsoon (Frey et al.
444 (2011); Weigel et al. (2011)) although based on a smaller data set of coincident CO and particle
445 detections. Moderately high or intermediate CO mixing ratios may result from the dilution of
446 young, CO-enriched air with aged and processed air masses, which would reduce both the CO
447 content of the air and its NPF precursor concentration. As soon as the thermodynamic
448 conditions for NPF are reached during transport, the formation process may be initialised, while
449 the content of diluted CO could indicate an unremarkable pollution state of the probed air. In air
450 masses with lowest CO content (~ 40 - 60 nmol mol^{-1}) NPF was observed only above the
451 tropopause (θ > 380 K) and in the absence of ice particles with n_{uf} ranging from 300 mg^{-1} to a
452 maximum of 2000 mg^{-1} (Weigel et al., 2020a).

https://doi.org/10.5194/acp-2020-1285
Preprint. Discussion started: 5 January 2021


Atmospheric Chemistry and Physics Discussions

Most intense NPF, i.e. with highest densities of ultrafine aerosol particles, were found below the tropopause (~ 380 K). In the presence of ice particles (as in clear air), elevated n_{uf} values were also encountered at low CO mixing ratios, below ~ 70 nmol mol^{-1}, at potential temperatures of 370 - 380 K. Under clear-air conditions, NPF occurs at much lower CO mixing ratios, which is shown by the n_{uf} vertical profile (Figure 3f). The results of Figure 3 indicate that NPF predominantly occurred in an altitude band between 350 K and 380 K (corresponding to ~ 8.5 – 16.5 km) with n_{uf} in the range of about 1000 to 50000 mg^{-1}. The n_{uf} values of NPF in ice clouds do generally not differ from those of NPF under clear-sky conditions.

3.3 Statistics of NPF events in the presence of ice particles

The frequency of NPF occurrence in coincidence with ice particles is illustrated in Figure 4. The upper panel (Figure 4a) exhibits the absolute occurrence frequency of number concentrations N_{uf} observed during NPF events. The graphs compile all measurements (more than 4600 samples of 1-Hz resolved data, cf. Table 1), which comply with the NPF criterion (black), for a comparison with clear-air NPF events (green) and those, which were coincidently detected with ice particles (red). At heights of in-cloud NPF observations (i.e. between 350 K and 380 K), the number concentrations of particles larger than the ultrafine mode, i.e. N_{15} and N_{65}, ranged (by median) at ~ 200 cm^{-3} < N_{15} < 1000 cm^{-3} (COPAS) and ~ 60 cm^{-3} < N_{65}< 150 cm^{-3} (UHSAS-A, Mahnke et al. (2020)). Two features are apparent:

1) Number concentrations N_{uf} of more than ~ 8000 cm^{-3} seem more frequently observed (about 1.5 times more often) in clear-air conditions. However, as the number of in-cloud NPF observations with N_{uf} > 8000 cm^{-3} is comparably low (≤ 10 encounters), the statistics is likely insufficient for drawing additional conclusions from this. Whether or not the presence of cloud ice confines the chance to detect very recent NPF (resulting in high N_{uf}), is discussed in Section 6.
2) For NPF in the presence of cloud ice, number concentrations N_{uf} between 1500 - 4000 cm^{-3} were observed about twice as often as under clear-air conditions (Figure 4b).

Plausibly, highest N_{uf} values are particularly found in the absence of deposition surfaces, which ice particles would provide. It seems, however, less understandable why NPF should generate a particular range of N_{uf} more frequently in the presence of cloud ice. Further discussion on this issue is provided in Section 6.

Until this point, the presence or absence of ice particles was distinguished by the criteria N_{ice} = 0 cm^{-3} or N_{ice} > 0 cm^{-3}, respectively. Figure 4b exhibits the occurrence frequency of N_{uf} with ice particles N_{ice} > 0 cm^{-3} normalised to the occurrence frequency of N_{uf} of all NPF events (black curve in Figure 4a). More than 75 % of observed NPF cases with 2000 cm^{-3} < N_{uf} < 4000 cm^{-3} (~ 200 samples) occurred while ice particles were present. In Figure 4c, the occurrence

https://doi.org/10.5194/acp-2020-1285
Preprint. Discussion started: 5 January 2021


Atmospheric Chemistry and Physics Discussions

488 frequencies of N_{uf} are compiled for various levels of N_{ice}, which were normalised to N_{uf} at
489 $N_{ice} > 0$ cm^{-3} (red curve in Figure 4a). Thresholds of N_{ice} are set with stepwise increasing number
490 concentrations (by one order of magnitude), to investigate whether the occurrence of NPF is
491 eventually confined or significantly influenced by the ice particle number density.

492 Although very faint, so called sub-visible cirrus clouds were found to comprise very small ice
493 particle number concentrations of 10^{-5} cm^{-3} (corresponding to 0.1 per litre, cf. Kübbeler et al.
494 (2011); Spreitzer et al. (2017)). Sub-visible cirrus clouds with $N_{ice} < 10^{-3}$ cm^{-3} are assumed to
495 have negligible influence on the NPF process, as is also to conclude from Figure 4c. Therefore, a
496 first threshold level is set to $N_{ice} > 10^{-3}$ cm^{-3} (magenta curve), followed by a second threshold at
497 $N_{ice} > 10^{-2}$ cm^{-3} (corresponding to 1 – 10 ice particles per litre, blue curve), which still represents
498 a comparatively small amount of N_{ice} within sub-visible cirrus clouds (cf. Thomas et al. (2002);
499 Peter et al. (2003); Davis et al. (2010); Frey et al. (2011)). The maximum observed N_{ice} reached
500 up to ~ 3 cm^{-3}. Concerning the frequency of observed N_{uf}, the difference between $N_{ice} > 0$ cm^{-3}
501 and $N_{ice} > 10^{-3}$ cm^{-3} appears negligibly small. This leaves to conclude, that elevated N_{uf} were
502 mostly observed coincidently with ice crystal number densities greater than 10^{-3} cm^{-3}. With
503 rising N_{ice} level (above 10^{-2} cm^{-3}), the occurrence frequency of the highest N_{uf} (> ~ 5000 cm^{-3})
504 decreased. When N_{ice} exceeds 10^{-1} cm^{-3}, the occurrence of $N_{uf} > 4500$ cm^{-3} is significantly reduced
505 and $N_{uf} > 8500$cm^{-3} were absent. At the highest observed N_{ice} of ~ 3 cm^{-3}, NPF with $N_{uf} > 250$ cm^{-3}
506 were not detected anymore.

507 Hence, events with highest NPF-rate seem to occur preferentially at lower ice particle
508 concentrations or in clear air. At a certain N_{ice} level (~ 3 cm^{-3}), the process of NPF seems to be
509 suppressed. This is in general agreement with earlier findings (Weigel et al., 2011), which
510 indicated the confinement of NPF by number densities above 2 cm^{-3} of cloud ice particles with
511 diameter larger than 2 µm. Among other incidents, a singularly observed event was discussed
512 (*ibid.*), during which NPF was very likely suppressed by the excessive presence of cloud ice
513 particles, which then, on leaving the cloud, re-emerged with amounts of ultrafine particles of
514 almost previously observed magnitude. Although an ultimate observational evidence is
515 currently lacking, however, these findings suggest that NPF is entirely prevented in cases when
516 N_{ice} substantially exceeds 2 - 3 cm^{-3}.

517 ## 4 In-cloud NPF related to *IWC* and cloud particle number densities

518 ### 4.1 The relationship between cloud ice and aerosols

519 Based on *in-situ* measurements over northern Australia and over West Africa, de Reus et al.
520 (2009) investigated the relationship between the number density of submicron aerosol particles
521 and the abundance of cloud particles at UT/LS levels. The authors provided aerosol and ice

https://doi.org/10.5194/acp-2020-1285
Preprint. Discussion started: 5 January 2021


Atmospheric Chemistry and Physics Discussions

522 particle number concentrations, which were averaged over the duration of various cloud
523 encounters in order to measure the fraction of submicrometre-sized particles that potentially
524 convert into cloud ice. Concerning the homogeneous ice nucleation process, a specific
525 relationship between the number concentration of aerosol and of ice particles cannot be
526 expected (Kärcher and Lohmann, 2002), whereas such a relationship is inherent in the ice
527 clouds' heterogeneous freezing process. From their analyses, de Reus et al. (2009) concluded
528 that a very similar range of ice-aerosol-ratios is observable in the convective outflow of ordinary
529 tropical convection (Australia) as well as of large, mesoscale convective systems (MCSs, West
530 Africa).

531 The measurements from StratoClim 2017 were compiled correspondingly to de Reus et al.
532 (2009) and are depicted in Figure 5. To ease the recognition of the relationship between the
533 measured number concentrations of ice particles and total aerosol (N_{10}), reference lines are
534 included in Figure 5, which indicate the number of encountered cloud particles per number of
535 submicrometre-sized aerosol particles. In addition to the density ratios of 1 : 300 and 1 : 30 000
536 (as in de Reus et al. (2009)), here also the 1 : 500 000 and the 1 : 5 000 000 ratios are marked.
537 The two panels in Figure 5 comprise the same data set of ice cloud encounters from
538 StratoClim 2017. The data were averaged over at least 10 seconds and over up to ~ 23 minutes.

539 Several occasions were identified by de Reus et al. (2009) when comparatively high ratios with
540 up to a few hundreds of aerosol particles remained non-activated per single ice particle. The
541 cloud ice – aerosol – ratios, which were found in the Asian monsoon's convective outflow region,
542 are in general agreement with previous observations (de Reus et al., 2009) most of which were
543 limited to the blue shaded area in Figure 5. In agreement with previous findings, total aerosol
544 numbers of significantly less than a few hundreds per single ice particle were not observed
545 during StratoClim 2017. Up to N_{10} of 700 cm^{-3} almost all StratoClim data result from
546 measurements at mean ambient temperatures colder than -75 °C (correspondingly to the
547 observations by de Reus et al. (2009), shaded area). Frequent observations were made at
548 aerosol concentrations below 1000 cm^{-3}. Compared to previous findings, however, the
549 StratoClim data set comprises a lot more observations at cloud ice – aerosol - ratios between
550 1 : 3 000 and 1 : 500 000, including frequent events of elevated aerosol number concentrations
551 (> 10^3 cm^{-3}). High total aerosol number concentrations of more than 6000 cm^{-3}, were observed
552 at *IWC* values mostly below 10 µmol mol^{-1} (i.e. log (*IWC,* µmol mol^{-1}) ≈ 1, Figure 5a). The majority
553 of observations were made at mean *IWC* values below ~ 300 µmol mol^{-1} (i.e. log (*IWC,* µmol mol^{-1}) ≈ 2.5), which largely minimises the probability that the measured N_{10} were impacted by
555 shattering artefacts from ice particles (cf. Appendix A). The majority of NPF occurrences (mostly
556 at ambient air temperatures between – 50 °C and – 80 °C) coincide with cloud ice – aerosol –

https://doi.org/10.5194/acp-2020-1285
Preprint. Discussion started: 5 January 2021


Atmospheric Chemistry and Physics Discussions

ratios between 1 : 3 000 and 1 : 500 000 (cf. Figure 5b). In particular, the abundance of in-cloud NPF concentrates between ratios of 1 : 30 000 and 1 : 500 000, which may not further surprise, as the large aerosol number concentrations are indicative to result from NPF. Concentrations N_{10} of more than 1000 cm^{-3} were not detected at ratios greater than 1 : 3 000. For N_{10} above 500 cm^{-3} and for cloud ice – aerosol - ratios smaller than 1 : 30 000, i.e. where elevated total aerosol concentrations mostly coincide with lower ice particles densities ($\sim 10^{-3} – 10^{-1}$ cm^{-3}), the observations predominantly occurred during NPF. However, cloud ice – aerosol – ratios greater than 1 : 3 000 were reached mostly in the absence of NPF.

As pointed out by de Reus et al. (2009), there are caveats inherent with this kind of analyses. The strength or efficiency of the aerosol activation is not straightforward to deduce from provided ratios of total aerosol and cloud particle numbers. Many interdependencies exist that may impact the illustrated relationship, such as

1) the altering of the aerosol particles (coagulation, condensation) or of the cloud elements (sedimentation) or
2) the mixing of air masses with different aerosol and/or variable vapour saturation characteristics (entrainment).

The ice formation process (*liquid origin* or *in-situ*) and the convection dynamics may additionally affect the relationship of cloud elements and interstitial aerosol. Assigning ultrafine particles of thousands per cm^3 (or more) to result from NPF is comparatively straightforward. In contrast, N_{uf} of a few 10 - 100 cm^{-3} are potentially filtered by the NPF criterion, and are probably not identified as NPF event, if detected at total aerosol concentrations (N_{10}) of comparable numbers. Apart from demonstrating the reproducibility of earlier findings (de Reus et al., 2009), the StratoClim mission allowed for extending this data set by new observations at different conditions, particularly by including NPF.

In essence, these findings confirm that the occurrence of NPF is constrained by the cloud ice microphysical properties such as particle size and number (both implied in the *IWC*). Total aerosol number concentrations N_{10} of a few hundreds per cubic centimetre were measured even at highest cloud particle number concentrations ($N_{ice} > 2 \cdot 10^{-1}$ cm^{-3}) whereas, under such conditions, NPF encounters remain exceptional. The following approach aims to narrow down the cloud particle microphysical properties that limits the occurrence of in-cloud NPF.

4.2 NPF in the *IWC*-*T* parameter space

Analyses in earlier cirrus-related studies concerning the clouds' ice water content (*IWC*) as a function of ambient air temperature provide insight into the processes inherent with the cirrus formation (Krämer et al., 2016). As introduced by Luebke et al. (2016), Krämer et al. (2016), and Wernli et al. (2016), a distinction of cirrus clouds regarding their formation mechanism is

https://doi.org/10.5194/acp-2020-1285
Preprint. Discussion started: 5 January 2021


Atmospheric Chemistry and Physics Discussions

592 obtainable within the *IWC-T* parameter space. The cirrus forms *in-situ* at elevated altitudes and
593 instantaneously at sufficiently cold temperatures. The *liquid-origin* cirrus cloud forms on
594 convective uplift from initially liquid droplets at lower altitudes (and less cold temperatures).
595 More specifically Wernli et al. (2016) distinguishes:

596 • *liquid-origin* cirrus: initially well-sized liquid cloud droplets freeze at almost
597 thermodynamic equilibrium in the ambient temperature range 235 K < T < 273 K under
598 nearly saturated conditions with respect to water (relative humidity RH_w of ~ 100 %)
599 but at high supersaturation with respect to ice ($RH_i \gg 100$ %), while at freezing level, the
600 water is capable to coexist in each of its phases (vapour, liquid, and ice).
601 • *in-situ* cirrus: under exclusion of pre-existing large liquid cloud droplets, ice crystals
602 nucleate heterogeneously (due to deposition freezing) or freeze homogeneously from
603 tiny supercooled aqueous solution droplets (Koop et al., 2000), which are designated as
604 "too small to be considered as cloud droplets" (Wernli et al., 2016).

605 The main goal of juxtaposing *IWC* and ambient air temperature is to investigate differences in
606 the characteristics of ice clouds, which may influence the cirrus clouds' radiative properties.
607 Additionally, those cirrus clouds' properties can be investigated, which arise from the dynamics
608 and conditions in which the cirrus ice particles have formed.

609 In Figure 6 the *IWCs* versus ambient air temperatures are displayed for all cloud encounters
610 throughout StratoClim 2017 as a function (colour code) of
611 a) the mixing ratio of ultrafine particles (i.e. $n_{6\text{-}15} = n_{uf}$; Figure 6a),
612 b) the total mixing ratio n_6 of particles with $d_p > 6$ nm (Figure 6b) and
613 c) the CO mixing ratio (Figure 6c), respectively.

614 The upper panel of Figure 6 includes two data sets: (1) all data from StratoClim 2017 in 1-Hz
615 resolution (grey data points) and (2) only the resulting n_{uf} complying with the NPF criterion
616 (colour coded data points). Mainly at very low ambient air temperatures (~ 200 K and colder)
617 and for comparatively high *IWC* values, the $n_{6\text{-}15}$ (grey) data were available but many failed the
618 NPF criterion. The absolute values of the mixing ratio n_6 of submicrometre-sized particles were
619 relatively high (Figure 6b). The detection of likewise excessive mixing ratios n_{15} (without
620 illustration) resulted in $n_{6\text{-}15}$, which did not exceed the threshold given with the NPF criterion (cf.
621 Section 1.1). Nevertheless, most of the $n_{6\text{-}15}$ data points, which failed the NPF criterion (cf. the
622 grey points in Figure 6a), coincide with the mixing ratios n_6 reaching up to several thousands of
623 mg^{-1}. It is not deducible from COPAS measurements how the enriched particle densities (n_6 and
624 n_{15}) distribute over the diameter spectrum of the submicrometre-sized aerosols. It therefore
625 remains open whether this observation is due to an expired NPF event with subsequent

https://doi.org/10.5194/acp-2020-1285
Preprint. Discussion started: 5 January 2021


Atmospheric Chemistry and Physics Discussions

626 coagulation of particles from the ultrafine size range (Weigel et al., 2020a), or whether the
627 particle enrichment is due to larger particles that were entered with the overshooting.

628 ● The absence of NPF at excessively high *IWC* within very cold air (Figure 6) suggests that NPF is
629 confined as soon as strong overshooting prevails, due to the presence of predominantly *liquid-*
630 *origin* ice particles. Excessive *IWC* (> 1000 µmol mol^{-1}) at air temperatures colder than 200 K
631 indicates that strong, vertically overshooting convection had occurred. These high *IWC* most
632 likely originated from cloud ice, which had formed at lower levels from liquid droplets. The
633 amount of water vapour that is required to form ice clouds of comparable *IWC* at these air
634 temperatures is too large to explain the formation of encountered cirrus by another than the
635 *liquid-origin* process. This feature was observed during the StratoClim flights on 27 July and on
636 10 August 2017. Within the same temperature range (T < 200 K), only a few NPF events with
637 moderately elevated n_{uf} of more than ~ 4000 mg^{-1} (log (n_{uf}, mg^{-1}) ≳ 3.6, yellow and reddish
638 colours in Figure 6a) were encountered offside from strong vertical overshooting.

639 ● In the presence of *in-situ* formed cirrus particles at cold temperatures, i.e. in or around the cold
640 point tropopause region, NPF events of remarkable strength (n_{uf} > 5000, i.e. log (n_{uf}, mg^{-1}) > 3.7,
641 orange and reddish colours in Figure 6a) or very recent NPF bursts were rarely observed. When
642 the cloud ice has likely formed *in-situ* (CO < 80 nmol mol^{-1}, yellow, greenish and blue colours in
643 Figure 6c), NPF of reduced strength was observed (n_{uf} < 1500 mg^{-1}, i.e. log (n_{uf}, mg^{-1}) < 3.2, bluish
644 colours of data points in Figure 6a). This indicates that NPF occurs in air with low CO content, i.e.
645 with comparatively low pollutant load.

646 ● Suppression of NPF by cloud particles (due to the number and size of ice particles) could
647 explain why the number of ultrafine particles remained below the NPF criterion threshold at
648 comparatively high *IWC*, albeit the total mixing ratios (n_6 or n_{15}) were significantly elevated. It is
649 not likely that a high number of interstitial, non-activated aerosol is accountable for the
650 abundance of submicrometre-sized particles. The large particle quantities observed (10^3 -
651 10^4 mg^{-1}) and the comparatively moderate CO content of the air sampled (≲ 100 nmol mol^{-1})
652 indicate a source of these particles at high altitudes. Very few hours after a completed NPF event
653 (≳ 4 h), however, the event may not be detectable anymore due to the short persistence of the
654 particles in the ultrafine size range (Weigel et al., 2020a). If the IWC values remained high over
655 several hours due to strong overshooting, and if NPF had happened more than four hours prior
656 to the measurements, then ultrafine particles could have coagulated to diameter sizes beyond
657 15 nm, hence, NPF would not have been identifiable anymore with COPAS.

658 ● The air's low pollutant load is indicated by comparatively moderate or low CO mixing ratios
659 between 50 and about 100 nmol mol^{-1} at ambient air temperatures of < 200 K (Figure 6c). For

https://doi.org/10.5194/acp-2020-1285
Preprint. Discussion started: 5 January 2021

Atmospheric Chemistry and Physics Discussions

comparison, the NPF observed during the West African monsoon were associated with CO levels between 60 and 90 nmol mol^{-1} (Weigel et al., 2011). Observation of moderate NPF (n_{uf} < 1500 mg^{-1}, log (n_{uf}, mg^{-1}) ≲ 3.3) in the midst of *in-situ* formed cloud ice in air with comparatively low pollutant load (CO < 80 nmol mol^{-1}) indicates that recent convective uplift of polluted air is not a prerequisite for NPF to occur. Slow processes, which cause an accumulation of NPF precursors at UT/LS altitudes, such as advection from elsewhere or the chemical and/or photo-chemical conversion, likely suffice to supply a reservoir of precursor material. In air with the highest CO content (> 100 nmol mol^{-1}), the *IWC*-*T*-values (for T > 200 K, i.e. at lower altitudes) remain in expected ranges and they scatter within the limits of most frequent observations (dashed black lines in Figure 6) as obtained from earlier analyses (Krämer et al., 2016). At the highest CO content (> 100 nmol mol^{-1}), the n_{uf} values remained predominantly below 5000 mg^{-1}.

5 The dependency of NPF on the proximity to ice particles

5.1 NPF as a function of mean free distance between ice elements

Surfaces, such as those of ice particles, represent a potential sink for the gaseous precursor species such as the H_2SO_4-H_2O system, since the ice particles' coating (Bogdan et al. (2006); Bogdan et al. (2013)) offers the necessary attachment points for the molecules of a condensable vapor. Consequently, an abundance of condensation surface should reduce or even prevent the NPF process. Cloud ice particles provide a comparatively large surface for coating, which raises the question whether NPF is affected by the presence of these particles.

The free distance between the ice particles is quantified based on the measurements of N_{ice} and of the ice particles' mean mass radius $\overline{r_{ice}}$, (consider $\overline{r_{ice}}^3 \sim \frac{IWC}{N_{ice}}$). The mean free volume in between the ice particles (the inter-crystal volume, *ICV* per cm^3 of air) is calculated with the number N^*_{ice} of ice particles per air volume (instead of the particles' number concentration) as:

$$\boldsymbol{ICV} = \frac{V - \frac{4}{3}\pi \cdot \bar{r}^3_{ice} \cdot N^*_{ice}}{N^*_{ice}} \qquad (2),$$

which basically subtracts the total ice volume from the sampled air volume (V = 1 cm^3) and the division by N^*_{ice} yields the *ICV*. Consequently, the *ICV* represents the mean particle-free volume assuming the distribution of ice crystals within the air volume as homogeneous. As long as the particle number and size remain small, subtracting the total ice volume from the air volume in equation (2) yields results without significant contribution. With a maximum of measured N^*_{ice} = 3 cm^{-3} together with the maximum detected ice particle radius of 100 µm, the subtraction $V - \frac{4}{3} \cdot \pi \cdot \bar{r}^3_{ice} \cdot N^*_{ice}$ corresponds to 1 cm^{-3} – 10^{-11} cm^{-3}. Hence, the volume of ice is insignificant

https://doi.org/10.5194/acp-2020-1285
Preprint. Discussion started: 5 January 2021

Atmospheric Chemistry and Physics Discussions

compared to the volume of air, and the *ICV* may be considered as a function of N_{ice} only. The mean inter-crystalline distance (*ICD,* in cm) is then calculated by:

$$\boldsymbol{ICD} = \sqrt[3]{\frac{\boldsymbol{ICV}}{\left(\frac{4}{3}\cdot\boldsymbol{\pi}\right)}} \qquad (3),$$

and the *ICV* is assumed as a sphere around every individual ice particle. The radius of each sphere constitutes the mean ice-free distance into any direction from the individual ice particle. Conceptually, this approach corresponds to the definition of the cloud elements' distance provided by Baumgartner and Spichtinger (2018).

Figure 7a depicts the number concentration of ultrafine particles (N_{uf}) as a function of the calculated ice particles' mean free distance from each other. The continuous colour transition of the data points from red to blue indicates the independence of the number of ultrafine particles in reference to the ice particles' mean free distance and rather documents the obvious relationship between the number of ice particles and their distance. The present ice particles compete for the limited amount of available water vapour; consequently, elevated number concentrations of ice particles are associated with many small ice particles. In essence, only the number of ice particles N_{ice} would not be able to constrain the occurrence and/or strength of NPF, as under encountered atmospheric conditions, a wide scattering of N_{uf} concentrations was observed at any *ICD* between about 1 cm and 10 cm.

Figure 7b shows the ice particles' mean mass radius $\overline{r_{ice}}$ as a function of the *ICD* and the number of ultrafine particles. By means of the mean mass radius $\overline{r_{ice}}$, two different cases were distinguished:

a) In the smallest ice particle size range ($\sim 3\,\mu m < \overline{r_{ice}} < \sim 20\,\mu m$, $\log(\overline{r_{ice}},\ \mu m) \lesssim 1.3$), a dependency of the *ICD* on the particle size was discernible. For instance, smallest ice particles (bluish $\overline{r_{ice}}$) predominantly coincided with short *ICD* of about 1 cm at elevated N_{ice}. Towards larger *ICD*, ice particle sizes continuously increased up to $\overline{r_{ice}} \approx 20\,\mu m$, which again reflects the competition of the ice crystals for the available water vapour. However, within the same interval of ice particle sizes ($\overline{r_{ice}} < \sim 20\,\mu m$), the concentrations N_{uf} scattered over almost two orders of magnitude (from $\sim 100\ cm^{-3}$ to $\sim 10\,000\ cm^{-3}$) up to *ICD* of ~ 10 cm without any obvious systematic.
b) In the presence of larger ice particles, $\overline{r_{ice}} > \sim 30\,\mu m$ ($1.3 < \log(\overline{r_{ice}},\ \mu m) \lesssim 1.4$, orange and reddish colours), the *ICD* ranged from ~ 1 cm to values above ~ 10 cm. Hence, not only $\overline{r_{ice}}$ determined the resulting *ICD,* but N_{ice} increasingly contributed as well. Unexpectedly, the concentrations N_{uf} were not at the highest when *ICD* values reached their maximum of slightly more than 10 cm. For largest particles sizes ($\overline{r_{ice}} > \sim 30\,\mu m$),

https://doi.org/10.5194/acp-2020-1285
Preprint. Discussion started: 5 January 2021


Atmospheric Chemistry and Physics Discussions

the values of N_{uf} accumulate at number concentrations of ~ 400 - 4000 cm^{-3} over the entire range of *ICDs*.

As long as the mean ice particle radius remained below a few dozen µm, NPF was encountered with almost any resulting N_{uf} concentration. It was shown before (Section 4.4 and Figure 4), that a wide scatter of N_{uf} was observed largely independent from coincidently detected number N_{ice} of ice particles. Hence, in-cloud NPF – as found during StratoClim 2017 - occurred almost unaffected by the ice particle number, as long as the mean ice particle size remained small enough (i.e. with $\overline{r_{ice}}$ < 20 µm).

Instead of evaluating the number of ultrafine particles as an exclusive function either of ice crystal number or of the ice particle radius, respectively, the *IWC* combines both microphysical parameters of the observed ice clouds, particle size and number concentration. The particle mass (i.e. the particle radius to the third power, r^3) is proportional to *IWC* and N_{ice}. Indeed, if N_{uf} over *ICD* are analysed as a function of *IWC,* a certain systematic becomes visible (Figure 7c). At lower *IWC* (< 1 µmol mol^{-1}, log (*IWC*, nmol mol^{-1}) ≲ 0, bluish and green colours) the *ICD*s were at the largest and observed NPF was of the highest intensity (N_{uf} of several thousands per cm^3). Between 1 µmol mol^{-1} and 10 µmol mol^{-1} (yellow colours) the maximum of N_{uf} throughout observed NPF events was reduced. The maximum N_{uf} was further reduced when *IWC* further increased beyond 10 µmol mol^{-1}. This result shows that the maximum N_{uf} reached throughout in-cloud NPF was determined by the combination of both, the ice particles' number concentration N_{ice} and their mean mass radius $\overline{r_{ice}}$.

5.2 NPF as a function of cloud elements' integral radius *IR*

Indications were found that both, number density and size of cloud ice particles, have a complementary effect on the amount of ultrafine particles (N_{uf}) resulting from in-cloud NPF. This motivates the compilation of N_{uf} values as a function of the integral radius $IR = \overline{r_{ice}} \cdot N_{ice}$ of the ice particle population. The parameter *IR* was described, e.g., by Manton (1979), or Politovich and Cooper (1988), and is frequently used to characterise clouds' microphysical properties (e.g. Korolev and Mazin (2003); or Krämer et al. (2009)). *IWC* and *IR* are expected to be strongly related as the diffusive growth of an ice particle is proportional to *IR* (see e.g. Pruppacher and Klett (2012)). The relationship between *IWC* and *IR* is also apparent from a systematic sorting of the data points displayed in Figure 8a. The probability should be high that weak NPF (generating low N_{uf}) often occurred in the presence of ice particles. In contrast, the occurrence of excessive NPF events in the cloud (with N_{uf} significantly exceeding several thousand per cm^3) was less likely. For almost all *IR* below 1 µm cm^{-3}, however, the N_{uf} concentrations were unsystematically scattered over the entire interval between ~ 100 cm^{-3} and ~ 10 000 cm^{-3}.

https://doi.org/10.5194/acp-2020-1285
Preprint. Discussion started: 5 January 2021

Atmospheric Chemistry and Physics Discussions

Towards the highest *IR* (> 1 µm cm^{-3}), the maximum of observed N_{uf} continuously decreased. Generally, this may reflect a limiting influence by the cloud ice on the maximum strength of occurring NPF (indicated by the diagonal grey-shaded bars in Figure 8). An exceptional feature is exhibited in Figure 8a with a high signal of N_{uf} (~ 3000 – 4000 cm^{-3}) amongst elevated *IR* (between ~ 4 and 10 µm cm^{-3}). This cluster of data points resulted from the measurements of two individual mission flights, on 27 July (~ 3000 cm^{-3} < N_{uf} < ~ 3500 cm^{-3}) and on 06 August (~ 3500 cm^{-3} < N_{uf} < ~ 4000 cm^{-3}), respectively. During these measuring periods, ice particle densities (N_{ice}) and the mean ice particle sizes (i.e. the particles' mean mass radius $\overline{r_{ice}}$) did not rise above 0.1 - 0.3 cm^{-3} and 25 - 50 µm. Neither N_{uf} nor the ice microphysics exceeded the range of moderate values. The two independent exceptional observations may indicate a local/temporal state of imbalance and could have been caused by:

1) moderate NPF, which was just proceeding when measured or which had been completed very recently (in such a case, the observed N_{uf} should rapidly decay due to coagulation, within less than one hour, to values of ~ 1000 cm^{-3}), or
2) ice particles, which sediment from high altitudes into an area of currently active NPF,
3) cooling of air accompanied with nucleation of ice, while the cooling is due to air parcel's vertical displacement possibly resulting from convective overshooting or gravity wave activity (cf. Weigel et al. 2020a).

The generally limiting influence by the cloud ice on the maximum strength of NPF, that is indicated by the majority of observations, is possibly explainable by the reduction of NPF precursors due to condensation onto present surfaces provided by the ice particles (maximum N_{ice}: 2 - 3 cm^{-3}). The question arises whether the distance between the ice particles allows efficient absorption and sustained reduction of NPF precursor molecules, or whether such an effect is only likely in the immediate vicinity of an ice particle. However, the effectiveness of such a process strongly depends on the diffusivity of the NPF precursor's molecules. If the molecules of the main NPF precursor are absorbed before thermodynamic conditions for NPF are reached, then these molecules are removed and missing in the formation of molecular clusters as initial step in the nucleation process. Sulphuric acid (H_2SO_4) is one of the most prominent condensable vapours and NPF precursors in the atmosphere. Numerical analyses concerning the reduction of the saturation ratio of H_2SO_4 due to the presence of ice particles, which are coated with H_2SO_4 (as typical for cirrus particles at 10-20 km altitude; cf. Bogdan et al. (2006); Bogdan et al. (2013)) are described in Appendix B: Impact of ice particles on NPF precursors' saturation ratio(see also Figure B- 1). Although the binary H_2SO_4-H_2O nucleation process alone is assumed as insufficient to explain atmospheric NPF (Bianchi et al. (2016); Kirkby et al. (2011)), the numerical analysis may qualitatively apply also for saturated condensable vapours containing compounds other than dissolved H_2SO_4 (Riccobono et al., 2014).

https://doi.org/10.5194/acp-2020-1285
Preprint. Discussion started: 5 January 2021


Atmospheric Chemistry and Physics Discussions

795 The numerical analysis yielded that the precursor's saturation ratio decreases rapidly with
796 increasing *IR*. As long as the ice particles' size remains small (radii < 10 µm) their influence on
797 the saturation ratio of the NPF precursor is comparatively weak. However, as demonstrated for
798 H_2SO_4 (cf. Appendix B), rising *IR* (combining ice particle size and number) could crucially confine
799 the production of high N_{uf}, or inhibit NPF at all. In particular, only completely uncoated ice
800 particles of pure water (which are excluded to exist in the UT/LS; cf. Bogdan et al. (2006);
801 Bogdan et al. (2013)) would be ineffective condensation surfaces for H_2SO_4 vapour, since
802 attachment points for H_2SO_4 molecules were lacking on the surface of pure ice water. Hence, the
803 frequent observations of in-cloud NPF is indicative for processes, which are capable of
804 maintaining sufficiently high NPF precursor saturation ratios. Such processes could involve
805 turbulent mixing of precursor-enriched air (entrainment) or a cooling process as induced, e.g. by
806 a temperature anomaly due to gravity wave activity (cf. Weigel et al. (2020a)). Otherwise, NPF
807 observations should be less frequently observable in the view of ice particles' effective influence
808 on the saturation ratio of NPF precursors.

809 From the results shown in Figure 8a, it may be concluded that the N_{uf}-range of 500-3000 cm^{-3} is
810 most frequently observed over the entire extent of detected *IR* values. While this confirms the
811 impression from Figure 4 (cf. Section 4.4), the conclusions from Figure 8 allow for approaching a
812 possible explanation of the N_{uf}'s behaviour with *IR*:

813 1) The maximum N_{uf} resulting from in-cloud NPF is determined by *IR*. Abundant ice
814 particles of sufficient size are capable of reducing the saturation ratio of NPF precursors
815 within time scales ranging from half an hour to a few hours. Consequently, moderate or
816 weak NPF events with less excessive N_{uf} production may occur most frequently in the
817 presence of cloud ice. However, the probability to instrumentally identify weak events
818 decreases with decreasing N_{uf}.
819 2) Furthermore, coagulation also affects N_{uf} in time scales of a few to dozens of hours (cf.
820 Weigel et al. 2020a), very likely constituting the most efficient altering process of
821 ultrafine particles from NPF.

822 At the time of observation, the age and processing progress of the ultrafine particles are
823 unknown. Amongst the previously described effects, the temporal delay between the NPF event
824 and the measurement may have a crucial but unquantifiable impact on the actually observed N_{uf},
825 as the altering of ultrafine particles is very effective in time scales of a few hours (Weigel et al.
826 2020a). Hence, it is likely a matter of probability, that in-cloud NPF with moderately high N_{uf}
827 (e.g. 500-3000 cm^{-3}) is most frequently observed. According to the data compiled in Figure 8, *IR*
828 values of about 24 µm cm^{-3} (corresponding to N_{ice} of about 0.7-0.8 cm^{-3} and mean mass radii $\overline{r_{ice}}$
829 of about 32 µm) constituted in general the uppermost limit for in-cloud NPF observation during
830 StratoClim 2017.

https://doi.org/10.5194/acp-2020-1285
Preprint. Discussion started: 5 January 2021


Atmospheric Chemistry and Physics Discussions

Another processing of the same data set, i.e. N_{uf} as a function of *IR*, implies a data sorting by means of CO mixing ratio (Figure 8b). Apparently, none of the emerging samples, neither with highest N_{uf} nor with highest *IR*, was directly ascribable to polluted air, which was recently lifted from the surface. Strongest NPF (N_{uf} > 5000 cm^{-3}) were exclusively observed at CO mixing ratios ranging between ~ 90 and 100 nmol mol^{-1}, which indicates the air's moderate pollutant load or its moderate age. Alternatively, these CO values may reflect certain mixing states of air masses of significantly different age. In less polluted air (CO mixing ratios below~ 70 nmol mol^{-1}), the *IR* reaches the highest values (up to ~ 24 µm cm^{-3}) which were observed together with elevated *IWC* (up to ~750 µmol mol^{-1}, i.e. log (*IWC*, nmol mol^{-1}) ≈ 0.88). Within pristine air, cloud ice particles mostly likely form *in-situ*. It is conceivable, that the *in-situ* cloud ice formation and NPF happens simultaneously, potentially induced by the same process: e.g. by updraughts due to subjacent convection (pileus effect) or by (local) cooling due to gravity waves (cf. Weigel et al. 2020a). In such cases (CO < 70 nmol mol^{-1}), the observed N_{uf} are systematically lower than 1000 cm^{-3} and they mostly range at a few hundreds per cm^3.

Hence, air masses with low pollutant loads obviously contain sufficient amounts of precursor material to supply moderate NPF (100 cm^{-3} < N_{uf} < 1000 cm^{-3}) which may strengthen the hypothesis that air's pollutant load is not an essential prerequisite for the occurrence of most intense NPF (N_{uf} > 5000 cm^{-3} at *IR* < 1 µm cm^{-3}) in the UT/LS region. This differs from earlier findings from ground-based measurements at high mountain sites (at about 5 km altitude) in the Himalaya region (Venzac et al., 2008) or at the Jungfraujoch station (~ 3.5 km altitude) in the Swiss Alps (Bianchi et al., 2016) who attributed their frequent NPF observations to the advection of polluted air which rises up from the valleys towards the research stations. Williamson et al. (2019) made their very frequent NPF observations based on a very comprehensive data set of airborne *in-situ* measurements over both oceans, the Atlantic and the Pacific, i.e., in certain distance away from direct convective supply by industrial pollution. However, different atmospheric conditions and/or different chemical precursor species might play a role in the NPF processes occurring in the boundary layer or at UT/LS altitudes.

6 Summary and Conclusions

Between 27 July and 10 August 2017 the airborne StratoClim mission took place in Kathmandu, Nepal, comprising eight mission flights (~ 22.5 hours of COPAS measurement time above 10 km, $\theta \gtrsim 350$ K) up to altitudes of 20 km ($\theta \approx 475$ K) with the Russian high-altitude research aircraft M-55 *Geophysica*. The present analysis includes the description and discussion of New Particle Formation (NPF) in the presence of cloud ice particles as observed in the UT/LS region of the Asian Monsoon Anticyclone (AMA) over northern India, Nepal and Bangladesh. Elevated concentrations of ultrafine particles (N_{uf}) generated by NPF were observed in hitherto unexpected frequency together with ice particles (N_{ice} > 0 cm^{-3}) at altitudes between ~ 11 km

https://doi.org/10.5194/acp-2020-1285
Preprint. Discussion started: 5 January 2021


Atmospheric Chemistry and Physics Discussions

and 16 km (~ 355 - 385 K) and mainly at ambient temperatures colder than ~ 230 K. During StratoClim 2017, a total number of 104 in-cloud NPF events was observed over a total duration of 1 hour and 17 minutes (~ 5 % of the total data set, ~ 49 % of all observed NPF cases). Maximum concentrations of ultrafine particles of up to ~ 11000 cm^{-3} (≈ 50000 mg^{-1}) were detected coincidently with ice particles in concentrations N_{ice} of 0.05 – 0.1 cm^{-3} (correspondent to 50 - 100 ice particles per litre) at heights of approximately 15 km (~ 370 K).

Analyses of the StratoClim data set concerning the relationship between interstitial aerosol and the abundance of cloud particles in the UT/LS are consistent with the findings from earlier measurements (de Reus et al., 2009), and extended these by new observations under different conditions. When ice particles are abundant (N_{ice} > 0.5 cm^{-3}), total aerosol number concentrations (N_{10}) remain generally between ~ 200 cm^{-3} and 700 cm^{-3}. In agreement with earlier findings (de Reus et al., 2009), the ratio of ice particle number and the number of submicrometre-sized aerosols did not significantly rise above 300 aerosols per ice particle at low air temperatures (< 200 K). Intense NPF, generating ultrafine particles of several thousands per cm^3, decrease the ice particle – aerosol – ratio substantially. However, such intense NPF was not observed at ratios larger than 1:3000, which indicates that the presence of cloud ice imposes limitations to the occurrence of NPF.

In-cloud NPF appears confined in the presence of predominantly *liquid-origin* ice particles with increased ice water content resulting from strong convective overshooting. This is confirmed by coincidently measured CO content of the air sample: air's pollutant load and/or its recent surface contact do not determine the strength of in-cloud NPF. Otherwise, the most intensive NPF events should occur within air masses with highest CO content. When the cloud ice has formed *in-situ,* at low CO mixing ratios, NPF was observed although with reduced strength. However, it is not yet conclusively clarified whether the direct convective supply of precursor material from pollution in the boundary layer is an essential prerequisite for the occurrence of NPF in the UT/LS, or whether NPF together with the ice cloud formation are initialised in processed and diluted air masses. The observations suggest that sufficient amounts of NPF precursor accumulate at UT/LS altitude, which is not necessarily connected to air's recent vertical uplift. It remains speculative, and it should be subject of suitable numerical analyses, to which extent the vertically lifted ice particles themselves contribute as carrier for soluble NPF precursor gases such as SO_2, H_2SO_4, or others, e.g., if dissolved in the cloud elements' liquid phase at lower heights and if released again at TTL altitudes after the cloud ice has sublimated. Comparatively slow processes, as air mass transport from elsewhere or the chemical and/or photo-chemical conversion at elevated altitudes may suffice to supply the reservoir of NPF precursors at UT/LS altitudes. NPF of highest intensity, however, was observed at moderate CO

https://doi.org/10.5194/acp-2020-1285
Preprint. Discussion started: 5 January 2021


Atmospheric Chemistry and Physics Discussions

mixing ratios, indicating a moderate pollutant load, and a certain age or mixing state of the air mass. Intense NPF seems almost confined in strong convective updraughts (cf. Section 4.2), either because of the intense dynamics inherent with overshooting convection, or because the precursor's saturation ratio of recently uplifted air does not suffice for immediate NPF.

The occurrence of NPF is strongly dependent on the precursor's saturation ratio. Ice particles in sufficient number and size are well capable to reduce the saturation ratio of a NPF precursor such as H_2SO_4. This implies two conclusions: 1) in-cloud NPF is confined by abundant ice particles and 2) not only the number of ice particles limits the NPF occurrence but also the ice particles' size. The strength of in-cloud NPF most clearly depends on the integral radius *IR* ($= \overline{r_{ice}} \cdot N_{ice}$), the product of the ice particles number concentration and the ice particles' mean mass radius. The *IR* turned out as appropriate cloud ice related parameter to juxtapose with NPF data. Up to *IR* of ~ 1 µm cm^{-3} the occurrence of NPF of any strength (with $\sim 100 < N_{uf} < 10\,000$ cm^{-3}) seems independent on the presence of ice particles at all. At larger *IR* (> 1 µm cm^{-3}) the presence of ice particles limits the maximum of N_{uf} from NPF. This result refines earlier findings (Weigel et al., 2011) that mainly the number of ice particles would limit the occurrence of NPF.

The observations indicate that a N_{uf}-range of 500-3000 cm^{-3} was most frequently observed during in-cloud NPF. However, weak NPF generating only low N_{uf} may occur most frequently in the presence of cloud ice, whilst the probability to instrumentally identify such weak events decreases with decreasing N_{uf}. Additionally, coagulation affects large N_{uf} in time scales of a few to dozens of hours (cf. Weigel et al. 2020a). As a consequence, the supposedly preferred N_{uf}-range likely results from superimposed effects, and it may be a matter of probability and timing (delay between NPF event and observation) that the N_{uf}-range of 500-3000 cm^{-3} is most frequently observed in the presence of cloud ice.

At the moment of observation, the age of the ultrafine aerosol (the delay between the NPF burst and the instrumental detection) as well as the aerosol's processing history is unknown. While the aerosol's persistence in the ultrafine size range is limited, it is conceivable that the abundance of aerosols influences the local formation of ice particles, or that ice particles are coated by ultrafine aerosol material due to coagulation. Above certain sizes, the cloud ice elements are increasingly subject to sedimentation. At warmer ambient temperatures, the ice particles may sublimate. This could release the materials attributed to the initially NPF-generated ultrafine aerosol. It remains speculative whether or not, in terms of physico-chemical characteristics, the released aerosol material is comparable with the primary NPF-generated aerosol. However, the sublimation of coated ice particles and the release of aerosol material at intermediate altitudes could provide nuclei for entrainment and/or cloud formation. It remains

https://doi.org/10.5194/acp-2020-1285
Preprint. Discussion started: 5 January 2021


Atmospheric Chemistry and Physics Discussions

unquantified, however, whether NPF near the surface (cf. Venzac et al. (2008) or Bianchi et al. (2016)) or the NPF at UT/LS altitudes contribute at the most to the availability of cloud condensation nuclei (CCN), which are supposed to promote cloud formation (Andreae et al., 2018) at the cloud condensation levels. Most likely the specific source contributions to the abundance of available CCN are as variable as are the chemical species potentially involved in the NPF process.

Data availability:

The data shown in this study are available at the StratoClim campaign database at

https://stratoclim.icg.kfa-juelich.de/AfcMain/CampaignDataBase

or they may be provided by respective PI upon request.

Author contribution

RW evaluated the data, created the figures, and draughted the manuscript with contributions by CM, MB, MK, HT and PS. SB participated in the data analyses and the manuscript draughting. Numerical simulations concerning the impact of ice particles on the saturation ratio of H_2SO_4 were performed by MB with contributions by HT. MK, NS, AA and CR contributed with cloud microphysical and water vapour data, SV and FD'A took care of the CO data. The manuscript was critically reviewed by CM, MB, MK, PS, NS, AA, CR, SV, FD'A, HT, and SB.

Competing interests

The authors declare no competing interests.

Acknowledgements
The contributions from the workshops of the Max Planck Institute for Chemistry and of the Institute for Physics of the Atmosphere (Mainz University) were essential for this work. In particular, we acknowledge support of T. Böttger, M. Flanz, C. v. Glahn, H. Rott, and W. Schneider. Also acknowledged are the comprehensive and helpful discussions with M. Szakáll. We very much thank the crew of MDB (Myasishchev Design Bureau) and the M-55 *Geophysica* pilots. The extraordinary commitment of F. Stroh in realisation of the campaign and the leadership of the entire StratoClim project by M. Rex are gratefully acknowledged. Some of our research leading to the presented results received funding from the European Research Council under the European Union's Seventh Framework Program (FP/2007-2013)/ERC Grant Agreement No. 321040 (EXCATRO). The StratoClim project was funded by the EU (FP7/2007–2018 Grant No. 603557) and also supported by the German "Bundesministerium für Bildung und Forschung" (BMBF) under the joint ROMIC-project SPITFIRE (01LG1205A). M. Baumgartner acknowledges support by the DFG within the Transregional Collaborative Research CentreTRR165 "Waves to Weather", Project Z2. P. Spichtinger acknowledges support by the DFG within the research unit Multiscale Dynamics of Gravity Waves (MS-GWaves) through grant SP 1163/5-2. H. Tost acknowledges funding from the Carl-Zeiss foundation. We explicitly thank the officials of the Nepalese government authorities, research institutions and Tribhuvan Airport as well as of the German

https://doi.org/10.5194/acp-2020-1285
Preprint. Discussion started: 5 January 2021


Atmospheric Chemistry and Physics Discussions

Embassy for their extraordinary support and hospitality, which enabled our field campaign and research.

Appendix A: Exclusion of artefacts on NPF observation due to the presence of cloud ice

During the herein discussed NPF events, the detected total number concentration of cloud elements never exceeded ~2-3 cm^{-3}. Thus, the number density of cloud elements were always significantly smaller (at least by two orders of magnitude) compared to detected aerosol number concentrations. At ambient air temperatures much colder than 235 K (and as cold as 187 K), the clouds entirely consisted of ice particles. In other studies, however, the discussions on NPF are restricted to measurements under cloud-free (clear-air) conditions as the cloud particles are suspected to possibly impact onto the aircraft's hull or the aerosol inlet, this way possibly generating artefacts on the aerosol measurements (Williamson et al. (2019) referring to Weber et al. (1998)). Regarding the in-cloud NPF observations throughout StratoClim 2017, the following aspects are noteworthy:

1) At typical flight speeds of the M-55 *Geophysica* (154 ± 39 m s^{-1}), sub-micrometre-sized ice particles should negligibly be subject to impaction on parts of the aircraft structure (nose, wing's leading edge, etc.) as the particles are well capable to follow the air stream around such flow obstacles (Kulkarni et al., 2011). Furthermore, ice particles in the diameter size range of a few micrometre (i.e. 1 µm < d_p < 10 µm) likely sublimate in the congestion region upstream of any aircraft structure (e.g. the wings leading edge, or the aerosol inlet). Even though a single particle of the aforementioned size could randomly enter the COPAS aerosol inlet, the diffuser-type entry of the aerosol inlet leads to a deceleration of the air flow inside the probe head (Weigel et al., 2009) accompanied with a sudden temperature increase in the air sample (according to fluid dynamical simulations of the inlet flow; Weigel et al. (2009) and references therein). Hence, rapid sublimation of ice particles in the diameter size range of a few µm can be expected to occur inside the aerosol inlet of COPAS. The entry of the sample air into the inlet's second diffuser additionally reduces the sampling of ice particle fragments.
2) The number concentration of ice particles with diameter d_p > 10 µm mostly remained below 0.4 cm^{-3} when coincidently detected with NPF. On impact and shattering of a single ice particle of such a size, the number of generated fragments is estimated to range at about 10-100 per cm^3 (Korolev et al., 2013). Hence, to substantially affect the detected number concentration of ultrafine particles (on magnitude order of hundreds to up to ten thousands per cm^3), the number of ice particles possibly emanating from shattering appears too low.
3) The probability that ice particles hit the sharp edged tips of the COPAS aerosol inlet (Weigel et al., 2009) appears negligibly small. The impaction surface provided by the

https://doi.org/10.5194/acp-2020-1285
Preprint. Discussion started: 5 January 2021


Atmospheric Chemistry and Physics Discussions

COPAS aerosol inlet is mainly the inlet's ring-shaped entry with an opening diameter of ~ 7.3 mm and a wall thickness of ~ 100 µm. In the unlikely case that a single ice particle impact occurred, all generated fragments were required to endure the temperature rise within the inlet head (cf. first argument of this list) and the transport through the aerosol lines towards the COPAS detectors before they can cause any effect on the measurement.

An effect of shattered large ice particles on the detection of ultrafine aerosol particles is ultimately not excludable. However, despite the reference by Williamson et al. (2019) in this context, ice particle fragmentation was not described by Weber et al. (1998). The same authors discuss the influence on NPF detections due to fragmentation of supercooled liquid-water cloud droplets and suggest a careful discussion in such cases. In general, such an influence due to the fragmentation of ice particles was largely ruled out or estimated as much lower than that of liquid droplets (Weber et al., 1998). Concerning the analyses discussed herein, however, it seems a statistical exception that ice particle fragments emanating from shattered ice particles crucially affect the measurement of the numbers of ultrafine aerosol particles. Moreover, if the NPF detections were systematically affected by the presence of cloud ice, the observed quantities of ultrafine particles would probably feature systematic and larger differences during in-cloud measurements compared to clear-air observations. None of the described artefacts was observable in the data from StratoClim 2017.

Appendix B: Impact of ice particles on NPF precursors' saturation ratio

Calculations were made regarding the time scales in which the decrease of the supersaturation of H_2SO_4 vapour occurs in the presence of coated ice particles. These serve as estimates concerning the efficiency of the diffusional loss of condensable materials, i.e. of the process competing with the gas-to-particle conversion of these vapours. The molecules of condensable and saturated (or supersaturated) vapours condense onto available surfaces, such as provided e.g. by an ice particle, whereas the combination of molecules into stable clusters requires significantly supersaturated conditions to form new particles out of the gas phase. However, it seems plausible that in the closest vicinity of an ice particle the condensational loss of a precursor gas like sulphuric acid (H_2SO_4) predominates over the NPF process. For H_2SO_4, as a representative of the NPF precursors, the question arises how efficient the condensation of H_2SO_4 occurs onto provided surface. The molecules' mobility and the condensation efficiency of the H_2SO_4 molecules is mainly determined by their diffusivity under the given atmospheric conditions. The diffusivity of H_2SO_4 is about a factor of 0.2-0.5 of the diffusivity of water vapour (Tang et al., 2014). Consequently, the condensational deposition of H_2SO_4 onto the coated particles surface causes the saturation ratio of H_2SO_4 to decrease within the environment of the

https://doi.org/10.5194/acp-2020-1285
Preprint. Discussion started: 5 January 2021


Atmospheric Chemistry and Physics Discussions

ice particle, which likely suppresses the process of NPF within a certain range around the ice particle.

Presuming that the ice particles are coated with H_2SO_4 (Bogdan et al. (2006); Bogdan et al. (2013)), model simulations were performed to investigate the timescales within which the coated ice particles reduce various H_2SO_4 saturation ratios. The simulation results (shown in Figure B- 1) are based on constant ambient temperature ($T \approx 200$ K) and pressure ($p = 110$ hPa) conditions. For the same temperature conditions, the saturation vapour pressure p_{sat} of H_2SO_4 is calculated according to Vehkamäki et al. (2002). This way, the degree of supersaturation is deducible from the H_2SO_4 molecules concentrations reported for the CLOUD (Cosmics Leaving OUtdoor Droplets) chamber experiments (cf. Kürten (2019), and references therein). According to this study, and in agreement with other references (H. Gordon, School of Earth and Environment, Leeds University, UK, personal communications Oct. 2019), molecule concentrations of $10^6 - 10^7$ cm^{-3} are required in the CLOUD chamber at temperatures of 208 K to induce NPF with nucleation rates of $10^{-2} - 100$ cm^{-3} s^{-1} (read out from Fig. 4 in Kürten (2019)). Keeping possible wall effects of the laboratory experiments in mind, for the occurrence of NPF under real atmospheric conditions, the lower bound of required molecule concentrations (10^6 cm^{-3}) may suffice, with an uncertainty of a factor five (H. Gordon, School of Earth and Environment, Leeds University, UK, personal communications Oct. 2019). At an ambient temperature of 208 K, the molecule concentrations of $10^6 - 10^7$ H_2SO_4 cm^{-3} (Kürten, 2019) correspond to saturation ratios of about $S \approx 10 - 100$. The following analysis, however, comprises a much wider range of saturation ratios between 10 and up to 5000 to account for a higher sensitivity of the temperature dependency of S and for other nucleation rates than chosen for this study.

Based on the expression formulated by Tsagkogeorgas et al. (2017) with the saturation vapour pressure p_{sat} of H_2SO_4 (above a flat surface) and with an accommodation coefficient of $\alpha = 0.65$ (Pöschl et al., 1998), the ice particle's change of mass m per time unit is calculated by:

$$\frac{\mathrm{d}m}{\mathrm{d}t} = \frac{4\pi D r (S-1)}{\left(\frac{L}{RT}-1\right)\frac{L}{T}\frac{D}{K} + \frac{RT}{\alpha \cdot p_{sat}}} \qquad (B-1),$$

which conceptually represents the change of mass (size) of the particles, onto which the H_2SO_4 condenses and which is also consistent with the finding that cirrus cloud elements are coated with a H_2SO_4-H_2O layer (Bogdan et al. (2006); Bogdan et al. (2013)). The diffusivity of H_2SO_4 molecules in air is denoted with D, and K refers to the thermal conductivity of air, while R and R_a are the gas constants of H_2SO_4 and the air, respectively. However, since the particle growth of micrometre-sized ice particles due to condensation of H_2SO_4 molecules is negligible, the change

https://doi.org/10.5194/acp-2020-1285
Preprint. Discussion started: 5 January 2021

Atmospheric Chemistry and Physics Discussions

of particle mass is considered as the loss of H_2SO_4 mass from the gas phase to the particles. The resulting change of saturation ratio per time unit is given as:

$$\frac{dS}{dt} = -\frac{R}{R_a}\frac{p}{p_{sat}} N_{ice} \frac{dm}{dt} \quad (B-2),$$

with the latent heat of vaporisation which is assumed as constant:

$$L = \frac{67.59 \cdot 10^3 \text{ J mol}^{-1}}{M_{H2SO4}} \quad (B-3),$$

and N_{ice} constitutes the number density of ice particles. Here, the sulphuric acid's molar mass is M_{H2SO4} = 0.098078 kg mol^{-1}. Note, the combination of the equations B−2 and B−1 depicts that $\frac{dS}{dt} \sim r \cdot N_{ice}$, i.e. the temporal change of the precursor's saturation ratio is proportional to the integral radius *IR* considered in Section 5.2.

In Figure B- 1 the variability of two aspects is considered and in the panels (a-c) it is distinguished between three ice particle radii (1 µm, 10 µm, and 100 µm) and two different ice particle number concentrations (0.01 and 0.1 cm^{-3}). The study by Ueyama et al. (2020) revealed that ice particles (effective radii of about 15 µm) persist over 12 to 20 hours at convective outflow levels between 365 K and 370 K potential temperature in the 2017 AMA.

Based on the simulation, apparently, the largest particles (r_p = 100 µm) are capable to efficiently suppress the NPF process. Particles of this size and in highest concentrations of 0.1 cm^{-3} cause the saturation ratio to rapidly abate to saturation level (i.e. S = 1) within 20-50 minutes. Even at lower concentrations (0.01 cm^{-3}) of particles of 100 µm radius, the saturation ratio is efficiently reduced by more than 70 % within 1 hour. Particles of 10 µm radius and in concentrations of 0.1 cm^{-3} appear to be equally efficient in reducing the saturation ratio by ~ 70 % within 1 hour. Smaller number concentrations of the same particle size range, and smaller particles (r_p = 1 µm), in general, require considerably more time than 1 hour to significantly reduce the H_2SO_4 saturation ratio.

In essence, cloud ice particles are well capable to rapidly reduce the saturation ratio of H_2SO_4 and, very likely, also the saturation ratio of other condensable gases. The ranges of N_{ice} (0.01 - 0.1 cm^{-3}) and particle size (1 µm < r_p < 100 µm) considered in the simulation correspond to the characteristics of ice particles coincidently observed with NPF throughout the StatoClim 2017 mission (away from NPF higher concentrations and larger sizes were found, cf. Krämer et al. (2020)). About 71% of all ice cloud detections in coincidence with NPF had an *IR* (i.e. $\overline{r_{ice}} \cdot N_{ice}$) of less than 1 µm cm^{-3}, while only about 1.5 % of the ice particle samples reached *IR* values greater than 7.5 µm cm^{-3}; the maximum *IR* of 24 µm cm^{-3} was encountered once throughout the entire mission. In general, the cirrus cloud particles are expected as coated with a H_2SO_4/H_2O

https://doi.org/10.5194/acp-2020-1285
Preprint. Discussion started: 5 January 2021

layer (Bogdan et al. (2006); Bogdan et al. (2013)) onto which sulphuric acid can condense. However, impurities by weaker and substitutable acids (such as organic acids or HCl or HNO_3) also allow the H_2SO_4 uptake on the surface, which could reduce the gaseous H_2SO_4 concentration this way potentially suppressing NPF. Hence, in certain abundance the presence of cloud ice particles restrains the NPF process, when condensation prevails over the competing gas-to-particle conversion. The efficiency of condensation onto the ice particles' surface strongly depends on

1) the size and number concentration of cloud ice particles and,
2) on the time interval during which the conditions remain at least saturated.

For the numerical simulation of the saturation decay, an ice particle is assumed as entirely coated (consistent with Bogdan et al. (2006); Bogdan et al. (2013)) and the (real) ice particle's habit (e.g. asphericity, porosity, etc.) remains unconsidered. Sporadic updraughts, such as initialised by convective lifting well below the NPF level, or gravity waves could cause small-scaled expansion and cooling which increases the precursor's supersaturation (Weigel et al., 2020a). Hence, a certain concentration of H_2SO_4 molecules could exceed the supersaturation threshold for NPF, even in the presence of abundant cloud ice, as long as the NPF process occurs faster than the reduction of S due to the present ice.

References

Afchine, A., Rolf, C., Costa, A., Spelten, N., Riese, M., Buchholz, B., Ebert, V., Heller, R., Kaufmann, S., Minikin, A., Voigt, C., Zöger, M., Smith, J., Lawson, P., Lykov, A., Khaykin, S., and Krämer, M.: Ice particle sampling from aircraft - influence of the probing position on the ice water content, Atmos Meas Tech, 11, 4015-4031, 10.5194/amt-11-4015-2018, 2018.

Andreae, M. O., Afchine, A., Albrecht, R., Holanda, B. A., Artaxo, P., Barbosa, H. M. J., Borrmann, S., Cecchini, M. A., Costa, A., Dollner, M., Fütterer, D., Järvinen, E., Jurkat, T., Klimach, T., Konemann, T., Knote, C., Krämer, M., Krisna, T., Machado, L. A. T., Mertes, S., Minikin, A., Pöhlker, C., Pöhlker, M. L., Pöschl, U., Rosenfeld, D., Sauer, D., Schlager, H., Schnaiter, M., Schneider, J., Schulz, C., Spanu, A., Sperling, V. B., Voigt, C., Walser, A., Wang, J., Weinzierl, B., Wendisch, M., and Ziereis, H.: Aerosol characteristics and particle production in the upper troposphere over the Amazon Basin, Atmos Chem Phys, 18, 921-961, 10.5194/acp-18-921-2018, 2018.

Ball, S. M., Hanson, D. R., Eisele, F. L., and McMurry, P. H.: Laboratory studies of particle nucleation: Initial results for H_2SO_4, H_2O, and NH_3 vapors, J Geophys Res-Atmos, 104, 23709-23718, 10.1029/1999jd900411, 1999.

Barth, M. C., Stuart, A. L., and Skamarock, W. C.: Numerical simulations of the July 10, 1996, Stratospheric-Tropospheric Experiment: Radiation, Aerosols, and Ozone (STERAO)-Deep Convection experiment storm: Redistribution of soluble tracers, J Geophys Res-Atmos, 106, 12381-12400, Doi 10.1029/2001jd900139, 2001.

Baumgartner, M., and Spichtinger, P.: Towards a bulk approach to local interactions of hydrometeors, Atmos Chem Phys, 18, 2525-2546, 10.5194/acp-18-2525-2018, 2018.

https://doi.org/10.5194/acp-2020-1285
Preprint. Discussion started: 5 January 2021

1147 Baumgartner, M., Weigel, R., Achatz, U., Harvey, A. H., and Spichtinger, P.: Reappraising the
1148 appropriate calculation of a common meteorological quantity: Potential Temperature, Atmos.
1149 Chem. Phys. Discuss., 2020, 1-43, 10.5194/acp-2020-361, 2020.

1150 Benson, D. R., Erupe, M. E., and Lee, S. H.: Laboratory-measured H_2SO_4-H_2O-NH_3 ternary
1151 homogeneous nucleation rates: Initial observations, Geophys Res Lett, 36, Artn L15818

1152 10.1029/2009gl038728, 2009.

1153 Bianchi, F., Tröstl, J., Junninen, H., Frege, C., Henne, S., Hoyle, C. R., Molteni, U., Herrmann, E.,
1154 Adamov, A., Bukowiecki, N., Chen, X., Duplissy, J., Gysel, M., Hutterli, M., Kangasluoma, J.,
1155 Kontkanen, J., Kürten, A., Manninen, H. E., Münch, S., Peräkylä, O., Petäjä, T., Rondo, L.,
1156 Williamson, C., Weingartner, E., Curtius, J., Worsnop, D. R., Kulmala, M., Dommen, J., and
1157 Baltensperger, U.: New particle formation in the free troposphere: A question of chemistry and
1158 timing, Science, 352, 1109-1112, 10.1126/science.aad5456, 2016.

1159 Bogdan, A., Molina, M. J., Sassen, K., and Kulmala, M.: Formation of low-temperature cirrus from
1160 H_2SO_4/H_2O aerosol droplets, J Phys Chem A, 110, 12541-12542, 10.1021/jp065898e, 2006.

1161 Bogdan, A., Molina, M. J., Kulmala, M., Tenhu, H., and Loerting, T.: Solution coating around ice
1162 particles of incipient cirrus clouds, P Natl Acad Sci USA, 110, E2439-E2439,
1163 10.1073/pnas.1304471110, 2013.

1164 Borrmann, S., Kunkel, D., Weigel, R., Minikin, A., Deshler, T., Wilson, J. C., Curtius, J., Volk, C. M.,
1165 Homan, C. D., Ulanovsky, A., Ravegnani, F., Viciani, S., Shur, G. N., Belyaev, G. V., Law, K. S., and
1166 Cairo, F.: Aerosols in the tropical and subtropical UT/LS: in-situ measurements of submicron
1167 particle abundance and volatility, Atmos Chem Phys, 10, 5573-5592, 10.5194/acp-10-5573-
1168 2010, 2010.

1169 Clarke, A. D., and Kapustin, V. N.: A pacific aerosol survey. Part I: A decade of data on particle
1170 production, transport, evolution, and mixing in the troposphere, Journal of the Atmospheric
1171 Sciences, 59, 363-382, 10.1175/1520-0469(2002)059<0363:Apaspi>2.0.Co;2, 2002.

1172 Clerbaux, C., George, M., Turquety, S., Walker, K. A., Barret, B., Bernath, P., Boone, C., Borsdorff, T.,
1173 Cammas, J. P., Catoire, V., Coffey, M., Coheur, P. F., Deeter, M., De Maziere, M., Drummond, J.,
1174 Duchatelet, P., Dupuy, E., de Zafra, R., Eddounia, F., Edwards, D. P., Emmons, L., Funke, B., Gille, J.,
1175 Griffith, D. W. T., Hannigan, J., Hase, F., Hopfner, M., Jones, N., Kagawa, A., Kasai, Y., Kramer, I., Le
1176 Flochmoen, E., Livesey, N. J., Lopez-Puertas, M., Luo, M., Mahieu, E., Murtagh, D., Nedelec, P.,
1177 Pazmino, A., Pumphrey, H., Ricaud, P., Rinsland, C. P., Robert, C., Schneider, M., Senten, C., Stiller,
1178 G., Strandberg, A., Strong, K., Sussmann, R., Thouret, V., Urban, J., and Wiacek, A.: CO
1179 measurements from the ACE-FTS satellite instrument: data analysis and validation using
1180 ground-based, airborne and spaceborne observations, Atmos Chem Phys, 8, 2569-2594,
1181 10.5194/acp-8-2569-2008, 2008.

1182 Corti, T., Luo, B. P., de Reus, M., Brunner, D., Cairo, F., Mahoney, M. J., Martucci, G., Matthey, R.,
1183 Mitev, V., dos Santos, F. H., Schiller, C., Shur, G., Sitnikov, N. M., Spelten, N., Vossing, H. J.,
1184 Borrmann, S., and Peter, T.: Unprecedented evidence for deep convection hydrating the tropical
1185 stratosphere, Geophys Res Lett, 35, Artn L10810

1186 10.1029/2008gl033641, 2008.

1187 Costa, A., Meyer, J., Afchine, A., Luebke, A., Gunther, G., Dorsey, J. R., Gallagher, M. W., Ehrlich, A.,
1188 Wendisch, M., Baumgardner, D., Wex, H., and Kramer, M.: Classification of Arctic, midlatitude and
1189 tropical clouds in the mixed-phase temperature regime, Atmos Chem Phys, 17, 12219-12238,
1190 10.5194/acp-17-12219-2017, 2017.

https://doi.org/10.5194/acp-2020-1285
Preprint. Discussion started: 5 January 2021

Atmospheric Chemistry and Physics Discussions

1191 Crutzen, P. J., and Lawrence, M. G.: The impact of precipitation scavenging on the transport of
1192 trace gases: A 3-dimensional model sensitivity study, J Atmos Chem, 37, 81-112, Doi
1193 10.1023/A:1006322926426, 2000.

1194 Curtius, J., Weigel, R., Vössing, H. J., Wernli, H., Werner, A., Volk, C. M., Konopka, P., Krebsbach, M.,
1195 Schiller, C., Roiger, A., Schlager, H., Dreiling, V., and Borrmann, S.: Observations of meteoric
1196 material and implications for aerosol nucleation in the winter Arctic lower stratosphere derived
1197 from in situ particle measurements, Atmos Chem Phys, 5, 3053-3069, 10.5194/acp-5-3053-
1198 2005, 2005.

1199 Davis, S., Hlavka, D. L., Jensen, E. J., Rosenlof, K., Yang, Q., Schmidt, S., Borrmann, S., Frey, W.,
1200 Lawson, P., Voemel, H., and Bui, T. P.: In situ and lidar observations of tropopause subvisible
1201 cirrus clouds during TC4, Journal of Geophysical Research: Atmospheres, 115,
1202 10.1029/2009jd013093, 2010.

1203 de Reus, M., Krejci, R., Williams, J., Fischer, H., Scheele, R., and Strom, J.: Vertical and horizontal
1204 distributions of the aerosol number concentration and size distribution over the northern Indian
1205 Ocean, J Geophys Res-Atmos, 106, 28629-28641, Doi 10.1029/2001jd900017, 2001.

1206 de Reus, M., Borrmann, S., Bansemer, A., Heymsfield, A. J., Weigel, R., Schiller, C., Mitev, V., Frey,
1207 W., Kunkel, D., Kurten, A., Curtius, J., Sitnikov, N. M., Ulanovsky, A., and Ravegnani, F.: Evidence
1208 for ice particles in the tropical stratosphere from in-situ measurements, Atmos Chem Phys, 9,
1209 6775-6792, DOI 10.5194/acp-9-6775-2009, 2009.

1210 Dunne, E. M., Gordon, H., Kürten, A., Almeida, J., Duplissy, J., Williamson, C., Ortega, I. K., Pringle,
1211 K. J., Adamov, A., Baltensperger, U., Barmet, P., Benduhn, F., Bianchi, F., Breitenlechner, M., Clarke,
1212 A., Curtius, J., Dommen, J., Donahue, N. M., Ehrhart, S., Flagan, R. C., Franchin, A., Guida, R., Hakala,
1213 J., Hansel, A., Heinritzi, M., Jokinen, T., Kangasluoma, J., Kirkby, J., Kulmala, M., Kupc, A., Lawler, M.
1214 J., Lehtipalo, K., Makhmutov, V., Mann, G., Mathot, S., Merikanto, J., Miettinen, P., Nenes, A.,
1215 Onnela, A., Rap, A., Reddington, C. L. S., Riccobono, F., Richards, N. A. D., Rissanen, M. P., Rondo, L.,
1216 Sarnela, N., Schobesberger, S., Sengupta, K., Simon, M., Sipilä, M., Smith, J. N., Stozkhov, Y., Tomé,
1217 A., Tröstl, J., Wagner, P. E., Wimmer, D., Winkler, P. M., Worsnop, D. R., and Carslaw, K. S.: Global
1218 atmospheric particle formation from CERN CLOUD measurements, Science, 354, 1119-1124,
1219 10.1126/science.aaf2649, 2016.

1220 Duplissy, J., Merikanto, J., Franchin, A., Tsagkogeorgas, G., Kangasluoma, J., Wimmer, D.,
1221 Vuollekoski, H., Schobesberger, S., Lehtipalo, K., Flagan, R. C., Brus, D., Donahue, N. M.,
1222 Vehkamaki, H., Almeida, J., Amorim, A., Barmet, P., Bianchi, F., Breitenlechner, M., Dunne, E. M.,
1223 Guida, R., Henschel, H., Junninen, H., Kirkby, J., Kurten, A., Kupc, A., Maattanen, A., Makhmutov, V.,
1224 Mathot, S., Nieminen, T., Onnela, A., Praplan, A. P., Riccobono, F., Rondo, L., Steiner, G., Tome, A.,
1225 Walther, H., Baltensperger, U., Carslaw, K. S., Dommen, J., Hansel, A., Petaja, T., Sipila, M.,
1226 Stratmann, F., Vrtala, A., Wagner, P. E., Worsnop, D. R., Curtius, J., and Kulmala, M.: Effect of ions
1227 on sulfuric acid-water binary particle formation: 2. Experimental data and comparison with QC-
1228 normalized classical nucleation theory, J Geophys Res-Atmos, 121, 1752-1775,
1229 10.1002/2015jd023539, 2016.

1230 Ebert, M., Weigel, R., Kandler, K., Günther, G., Molleker, S., Grooß, J. U., Vogel, B., Weinbruch, S.,
1231 and Borrmann, S.: Chemical analysis of refractory stratospheric aerosol particles collected
1232 within the arctic vortex and inside polar stratospheric clouds, Atmos. Chem. Phys., 16, 8405-
1233 8421, 10.5194/acp-16-8405-2016, 2016.

1234 Ekman, A. M. L., Wang, C., Strom, J., and Krejci, R.: Explicit simulation of aerosol physics in a
1235 cloud-resolving model: Aerosol transport and processing in the free troposphere, Journal of the
1236 Atmospheric Sciences, 63, 682-696, Doi 10.1175/Jas3645.1, 2006.

https://doi.org/10.5194/acp-2020-1285
Preprint. Discussion started: 5 January 2021

Atmospheric Chemistry and Physics Discussions

Frey, W., Borrmann, S., Kunkel, D., Weigel, R., de Reus, M., Schlager, H., Roiger, A., Voigt, C., Hoor, P., Curtius, J., Kramer, M., Schiller, C., Volk, C. M., Homan, C. D., Fierli, F., Di Donfrancesco, G., Ulanovsky, A., Ravegnani, F., Sitnikov, N. M., Viciani, S., D'Amato, F., Shur, G. N., Belyaev, G. V., Law, K. S., and Cairo, F.: In situ measurements of tropical cloud properties in the West African Monsoon: upper tropospheric ice clouds, Mesoscale Convective System outflow, and subvisual cirrus, Atmos Chem Phys, 11, 5569-5590, DOI 10.5194/acp-11-5569-2011, 2011.

Gordon, H., Kirkby, J., Baltensperger, U., Bianchi, F., Breitenlechner, M., Curtius, J., Dias, A., Dommen, J., Donahue, N. M., Dunne, E. M., Duplissy, J., Ehrhart, S., Flagan, R. C., Frege, C., Fuchs, C., Hansel, A., Hoyle, C. R., Kulmala, M., Kürten, A., Lehtipalo, K., Makhmutov, V., Molteni, U., Rissanen, M. P., Stozkhov, Y., Tröstl, J., Tsagkogeorgas, G., Wagner, R., Williamson, C., Wimmer, D., Winkler, P. M., Yan, C., and Carslaw, K. S.: Causes and importance of new particle formation in the present-day and preindustrial atmospheres, Journal of Geophysical Research: Atmospheres, 122, 8739-8760, 10.1002/2017jd026844, 2017.

He, Q., Ma, J., Zheng, X., Yan, X., Vömel, H., Wienhold, F. G., Gao, W., Liu, D., Shi, G., and Cheng, T.: Observational evidence of particle hygroscopic growth in the upper troposphere–lower stratosphere (UTLS) over the Tibetan Plateau, Atmos. Chem. Phys., 19, 8399-8406, 10.5194/acp-19-8399-2019, 2019.

Höpfner, M., Ungermann, J., Borrmann, S., Wagner, R., Spang, R., Riese, M., Stiller, G., Appel, O., Batenburg, A. M., Bucci, S., Cairo, F., Dragoneas, A., Friedl-Vallon, F., Hünig, A., Johansson, S., Krasauskas, L., Legras, B., Leisner, T., Mahnke, C., Möhler, O., Molleker, S., Müller, R., Neubert, T., Orphal, J., Preusse, P., Rex, M., Saathoff, H., Stroh, F., Weigel, R., and Wohltmann, I.: Ammonium nitrate particles formed in upper troposphere from ground ammonia sources during Asian monsoons, Nat Geosci, 12, 608-612, 10.1038/s41561-019-0385-8, 2019.

Jost, A., Szakáll, M., Diehl, K., Mitra, S. K., and Borrmann, S.: Chemistry of riming: the retention of organic and inorganic atmospheric trace constituents, Atmos. Chem. Phys., 17, 9717-9732, 10.5194/acp-17-9717-2017, 2017.

Kärcher, B., and Lohmann, U.: A parameterization of cirrus cloud formation: Homogeneous freezing of supercooled aerosols, J Geophys Res-Atmos, 107, 4010, 10.1029/2001jd000470, 2002.

Kazil, J., Lovejoy, E. R., Jensen, E. J., and Hanson, D. R.: Is aerosol formation in cirrus clouds possible?, Atmos Chem Phys, 7, 1407-1413, DOI 10.5194/acp-7-1407-2007, 2007.

Kazil, J., Harrison, R. G., and Lovejoy, E. R.: Tropospheric new particle formation and the role of ions, Space Sci Rev, 137, 241-255, 10.1007/s11214-008-9388-2, 2008.

Kerminen, V. M., Chen, X. M., Vakkari, V., Petäjä, T., Kulmala, M., and Bianchi, F.: Atmospheric new particle formation and growth: review of field observations, Environ Res Lett, 13, Artn 103003

10.1088/1748-9326/Aadf3c, 2018.

Kirkby, J., Curtius, J., Almeida, J., Dunne, E., Duplissy, J., Ehrhart, S., Franchin, A., Gagne, S., Ickes, L., Kurten, A., Kupc, A., Metzger, A., Riccobono, F., Rondo, L., Schobesberger, S., Tsagkogeorgas, G., Wimmer, D., Amorim, A., Bianchi, F., Breitenlechner, M., David, A., Dommen, J., Downard, A., Ehn, M., Flagan, R. C., Haider, S., Hansel, A., Hauser, D., Jud, W., Junninen, H., Kreissl, F., Kvashin, A., Laaksonen, A., Lehtipalo, K., Lima, J., Lovejoy, E. R., Makhmutov, V., Mathot, S., Mikkila, J., Minginette, P., Mogo, S., Nieminen, T., Onnela, A., Pereira, P., Petaja, T., Schnitzhofer, R., Seinfeld, J. H., Sipila, M., Stozhkov, Y., Stratmann, F., Tome, A., Vanhanen, J., Viisanen, Y., Vrtala, A., Wagner, P. E., Walther, H., Weingartner, E., Wex, H., Winkler, P. M., Carslaw, K. S., Worsnop, D. R.,

https://doi.org/10.5194/acp-2020-1285
Preprint. Discussion started: 5 January 2021

1281 Baltensperger, U., and Kulmala, M.: Role of sulphuric acid, ammonia and galactic cosmic rays in
1282 atmospheric aerosol nucleation, Nature, 476, 429-U477, 10.1038/nature10343, 2011.

1283 Koop, T., Luo, B. P., Tsias, A., and Peter, T.: Water activity as the determinant for homogeneous
1284 ice nucleation in aqueous solutions, Nature, 406, 611-614, Doi 10.1038/35020537, 2000.

1285 Korolev, A., Emery, E., and Creelman, K.: Modification and tests of particle probe tips to mitigate
1286 effects of ice shattering, Journal of Atmospheric and Oceanic Technology, 30, 690-708,
1287 10.1175/JTECH-D-12-00142.1, 2013.

1288 Korolev, A. V., and Mazin, I. P.: Supersaturation of Water Vapor in Clouds, Journal of the
1289 Atmospheric Sciences, 60, 2957-2974, 10.1175/1520-0469(2003)060<2957:sowvic>2.0.co;2,
1290 2003.

1291 Krämer, M., Schiller, C., Afchine, A., Bauer, R., Gensch, I., Mangold, A., Schlicht, S., Spelten, N.,
1292 Sitnikov, N., Borrmann, S., de Reus, M., and Spichtinger, P.: Ice supersaturations and cirrus cloud
1293 crystal numbers, Atmos Chem Phys, 9, 3505-3522, 2009.

1294 Krämer, M., Rolf, C., Luebke, A., Afchine, A., Spelten, N., Costa, A., Meyer, J., Zöger, M., Smith, J.,
1295 Herman, R. L., Buchholz, B., Ebert, V., Baumgardner, D., Borrmann, S., Klingebiel, M., and
1296 Avallone, L.: A microphysics guide to cirrus clouds - Part 1: Cirrus types, Atmospheric Chemistry
1297 and Physics, 16, 3463-3483, 10.5194/acp-16-3463-2016, 2016.

1298 Krämer, M., Rolf, C., Spelten, N., Afchine, A., Fahey, D., Jensen, E., Khaykin, S., Kuhn, T., Lawson, P.,
1299 Lykov, A., Pan, L. L., Riese, M., Rollins, A., Stroh, F., Thornberry, T., Wolf, V., Woods, S., Spichtinger,
1300 P., Quaas, J., and Sourdeval, O.: A microphysics guide to cirrus – Part 2: Climatologies of clouds
1301 and humidity from observations, Atmos. Chem. Phys., 20, 12569-12608, 10.5194/acp-20-12569-
1302 2020, 2020.

1303 Kübbeler, M., Hildebrandt, M., Meyer, J., Schiller, C., Hamburger, T., Jurkat, T., Minikin, A., Petzold,
1304 A., Rautenhaus, M., Schlager, H., Schumann, U., Voigt, C., Spichtinger, P., Gayet, J. F., Gourbeyre, C.,
1305 and Krämer, M.: Thin and subvisible cirrus and contrails in a subsaturated environment, Atmos
1306 Chem Phys, 11, 5853-5865, 10.5194/acp-11-5853-2011, 2011.

1307 Kulkarni, P., Baron, P. A., and Willeke, K.: Aerosol measurement: principles, techniques, and
1308 applications, John Wiley & Sons, 2011.

1309 Kürten, A., Williamson, C., Almeida, J., Kirkby, J., and Curtius, J.: On the derivation of particle
1310 nucleation rates from experimental formation rates, Atmos Chem Phys, 15, 4063-4075,
1311 10.5194/acp-15-4063-2015, 2015.

1312 Kürten, A., Bianchi, F., Almeida, J., Kupiainen-Maatta, O., Dunne, E. M., Duplissy, J., Williamson, C.,
1313 Barmet, P., Breitenlechner, M., Dommen, J., Donahue, N. M., Flagan, R. C., Franchin, A., Gordon, H.,
1314 Hakala, J., Hansel, A., Heinritzi, M., Ickes, L., Jokinen, T., Kangasluoma, J., Kim, J., Kirkby, J., Kupc,
1315 A., Lehtipalo, K., Leiminger, M., Makhmutov, V., Onnela, A., Ortega, I. K., Petaja, T., Praplan, A. P.,
1316 Riccobono, F., Rissanen, M. P., Rondo, L., Schnitzhofer, R., Schobesberger, S., Smith, J. N., Steiner,
1317 G., Stozhkov, Y., Tome, A., Trostl, J., Tsagkogeorgas, G., Wagner, P. E., Wimmer, D., Ye, P. L.,
1318 Baltensperger, U., Carslaw, K., Kulmala, M., and Curtius, J.: Experimental particle formation rates
1319 spanning tropospheric sulfuric acid and ammonia abundances, ion production rates, and
1320 temperatures, J Geophys Res-Atmos, 121, 12377-12400, 10.1002/2015jd023908, 2016.

1321 Kürten, A.: New particle formation from sulfuric acid and ammonia: nucleation and growth
1322 model based on thermodynamics derived from CLOUD measurements for a wide range of
1323 conditions, Atmos. Chem. Phys., 19, 5033-5050, 10.5194/acp-19-5033-2019, 2019.

https://doi.org/10.5194/acp-2020-1285
Preprint. Discussion started: 5 January 2021

Atmospheric Chemistry and Physics Discussions

1324 Lee, S. H., Reeves, J. M., Wilson, J. C., Hunton, D. E., Viggiano, A. A., Miller, T. M., Ballenthin, J. O.,
1325 and Lait, L. R.: Particle formation by ion nucleation in the upper troposphere and lower
1326 stratosphere, Science, 301, 1886-1889, DOI 10.1126/science.1087236, 2003.

1327 Lee, S. H., Wilson, J. C., Baumgardner, D., Herman, R. L., Weinstock, E. M., LaFleur, B. G., Kok, G.,
1328 Anderson, B., Lawson, P., Baker, B., Strawa, A., Pittman, J. V., Reeves, J. M., and Bui, T. P.: New
1329 particle formation observed in the tropical/subtropical cirrus clouds, J Geophys Res-Atmos, 109,
1330 Artn D20209

1331 10.1029/2004jd005033, 2004.

1332 Logan, J. A., Prather, M. J., Wofsy, S. C., and Mcelroy, M. B.: Tropospheric Chemistry - a Global
1333 Perspective, J Geophys Res-Oceans, 86, 7210-7254, DOI 10.1029/JC086iC08p07210, 1981.

1334 Lovejoy, E. R., Curtius, J., and Froyd, K. D.: Atmospheric ion-induced nucleation of sulfuric acid
1335 and water, J Geophys Res-Atmos, 109, Artn D08204

1336 10.1029/2003jd004460, 2004.

1337 Luebke, A. E., Afchine, A., Costa, A., Grooss, J. U., Meyer, J., Rolf, C., Spelten, N., Avallone, L. M.,
1338 Baumgardner, D., and Krämer, M.: The origin of midlatitude ice clouds and the resulting
1339 influence on their microphysical properties, Atmos Chem Phys, 16, 5793-5809, 10.5194/acp-16-
1340 5793-2016, 2016.

1341 Mahnke, C., Weigel, R., Cairo, F., Vernier, J.-P., Afchine, A., Krämer, M., Mitev, V., Matthey, R.,
1342 Viciani, S., D'Amato, F., Ploeger, F., Deshler, T., and Borrmann, S.: The ATAL within the 2017
1343 Asian Monsoon Anticyclone: Microphysical aerosol properties derived from aircraft-borne in
1344 situ measurements, Atmos. Chem. Phys. Discuss., acp-2020-1241 2020.

1345 Manton, M. J.: On the broadening of a droplet distribution by turbulence near cloud base, Q J Roy
1346 Meteor Soc, 105, 899-914, 10.1002/qj.49710544613, 1979.

1347 Merikanto, J., Spracklen, D. V., Mann, G. W., Pickering, S. J., and Carslaw, K. S.: Impact of nucleation
1348 on global CCN, Atmos Chem Phys, 9, 8601-8616, 10.5194/acp-9-8601-2009, 2009.

1349 Meyer, J., Rolf, C., Schiller, C., Rohs, S., Spelten, N., Afchine, A., Zöger, M., Sitnikov, N., Thornberry,
1350 T. D., Rollins, A. W., Bozoki, Z., Tatrai, D., Ebert, V., Kuhnreich, B., Mackrodt, P., Möhler, O.,
1351 Saathoff, H., Rosenlof, K. H., and Krämer, M.: Two decades of water vapor measurements with the
1352 FISH fluorescence hygrometer: a review, Atmos Chem Phys, 15, 8521-8538, 10.5194/acp-15-
1353 8521-2015, 2015.

1354 Pan, L. L., Honomichl, S. B., Kinnison, D. E., Abalos, M., Randel, W. J., Bergman, J. W., and Bian, J.:
1355 Transport of chemical tracers from the boundary layer to stratosphere associated with the
1356 dynamics of the Asian summer monsoon, Journal of Geophysical Research: Atmospheres, 121,
1357 14.159-114.174, 10.1002/2016jd025616, 2016.

1358 Park, M., Randel, W. J., Gettelman, A., Massie, S. T., and Jiang, J. H.: Transport above the Asian
1359 summer monsoon anticyclone inferred from Aura Microwave Limb Sounder tracers, J Geophys
1360 Res-Atmos, 112, Artn D16309

1361 10.1029/2006jd008294, 2007.

1362 Park, M., Randel, W. J., Emmons, L. K., and Livesey, N. J.: Transport pathways of carbon monoxide
1363 in the Asian summer monsoon diagnosed from Model of Ozone and Related Tracers (MOZART), J
1364 Geophys Res-Atmos, 114, Artn D08303

https://doi.org/10.5194/acp-2020-1285
Preprint. Discussion started: 5 January 2021

Atmospheric Chemistry and Physics Discussions

10.1029/2008jd010621, 2009.

Peter, T., Luo, B. P., Wirth, M., Kiemle, C., Flentje, H., Yushkov, V. A., Khattatov, V., Rudakov, V., Thomas, A., Borrmann, S., Toci, G., Mazzinghi, P., Beuermann, J., Schiller, C., Cairo, F., Di Donfrancesco, G., Adriani, A., Volk, C. M., Strom, J., Noone, K., Mitev, V., MacKenzie, R. A., Carslaw, K. S., Trautmann, T., Santacesaria, V., and Stefanutti, L.: Ultrathin Tropical Tropopause Clouds (UTTCs): I. Cloud morphology and occurrence, Atmos. Chem. Phys., 3, 1083-1091, 10.5194/acp-3-1083-2003, 2003.

Ploeger, F., Günther, G., Konopka, P., Fueglistaler, S., Müller, R., Hoppe, C., Kunz, A., Spang, R., Grooss, J. U., and Riese, M.: Horizontal water vapor transport in the lower stratosphere from subtropics to high latitudes during boreal summer, J Geophys Res-Atmos, 118, 8111-8127, 10.1002/jgrd.50636, 2013.

Ploeger, F., Gottschling, C., Griessbach, S., Grooss, J. U., Günther, G., Konopka, P., Müller, R., Riese, M., Stroh, F., Tao, M., Ungermann, J., Vogel, B., and von Hobe, M.: A potential vorticity-based determination of the transport barrier in the Asian summer monsoon anticyclone, Atmos Chem Phys, 15, 13145-13159, 10.5194/acp-15-13145-2015, 2015.

Politovich, M. K., and Cooper, W. A.: Variability of the Supersaturation in Cumulus Clouds, Journal of the Atmospheric Sciences, 45, 1651-1664, 10.1175/1520-0469(1988)045<1651:votsic>2.0.co;2, 1988.

Pöschl, U., Canagaratna, M., Jayne, J. T., Molina, L. T., Worsnop, D. R., Kolb, C. E., and Molina, M. J.: Mass Accommodation Coefficient of H_2SO_4 Vapor on Aqueous Sulfuric Acid Surfaces and Gaseous Diffusion Coefficient of H_2SO_4 in N_2/H_2O, The Journal of Physical Chemistry A, 102, 10082-10089, 10.1021/jp982809s, 1998.

Pruppacher, H. R., and Klett, J. D.: Microphysics of Clouds and Precipitation: Reprinted 1980, Springer Science & Business Media, 2012.

Randel, W. J., and Park, M.: Deep convective influence on the Asian summer monsoon anticyclone and associated tracer variability observed with Atmospheric Infrared Sounder (AIRS), J Geophys Res-Atmos, 111, Artn D12314

10.1029/2005jd006490, 2006.

Riccobono, F., Schobesberger, S., Scott, C. E., Dommen, J., Ortega, I. K., Rondo, L., Almeida, J., Amorim, A., Bianchi, F., Breitenlechner, M., David, A., Downard, A., Dunne, E. M., Duplissy, J., Ehrhart, S., Flagan, R. C., Franchin, A., Hansel, A., Junninen, H., Kajos, M., Keskinen, H., Kupc, A., Kürten, A., Kvashin, A. N., Laaksonen, A., Lehtipalo, K., Makhmutov, V., Mathot, S., Nieminen, T., Onnela, A., Petaja, T., Praplan, A. P., Santos, F. D., Schallhart, S., Seinfeld, J. H., Sipila, M., Spracklen, D. V., Stozhkov, Y., Stratmann, F., Tome, A., Tsagkogeorgas, G., Vaattovaara, P., Viisanen, Y., Vrtala, A., Wagner, P. E., Weingartner, E., Wex, H., Wimmer, D., Carslaw, K. S., Curtius, J., Donahue, N. M., Kirkby, J., Kulmala, M., Worsnop, D. R., and Baltensperger, U.: Oxidation Products of Biogenic Emissions Contribute to Nucleation of Atmospheric Particles, Science, 344, 717-721, 10.1126/science.1243527, 2014.

Schulz, C., Schneider, J., Holanda, B. A., Appel, O., Costa, A., de Sa, S. S., Dreiling, V., Fütterer, D., Jurkat-Witschas, T., Klimach, T., Knote, C., Krämer, M., Martin, S. T., Mertes, S., Pöhlker, M. L., Sauer, D., Voigt, C., Walser, A., Weinzierl, B., Ziereis, H., Zöger, M., Andreae, M. O., Artaxo, P., Machado, L. A. T., Pöschl, U., Wendisch, M., and Borrmann, S.: Aircraft-based observations of isoprene-epoxydiol-derived secondary organic aerosol (IEPOX-SOA) in the tropical upper troposphere over the Amazon region, Atmos Chem Phys, 18, 14979-15001, 10.5194/acp-18-14979-2018, 2018.

https://doi.org/10.5194/acp-2020-1285
Preprint. Discussion started: 5 January 2021

1410 Schumann, U., Kiemle, C., Schlager, H., Weigel, R., Borrmann, S., D'Amato, F., Krämer, M., Matthey,
1411 R., Protat, A., Voigt, C., and Volk, C. M.: Long-lived contrails and convective cirrus above the
1412 tropical tropopause, Atmos. Chem. Phys., 17, 2311-2346, 10.5194/acp-17-2311-2017, 2017.

1413 Sokolov, L., and Lepuchov, B.: Protocol of interaction between Unit for Connection with Scientific
1414 Equipment (UCSE) and on-board scientific equipment of Geophysica aircraft (Second edition),
1415 Myasishchev Design Bureau (MDB), 1998.

1416 Spracklen, D. V., Carslaw, K. S., Kulmala, M., Kerminen, V. M., Mann, G. W., and Sihto, S. L.: The
1417 contribution of boundary layer nucleation events to total particle concentrations on regional and
1418 global scales, Atmos Chem Phys, 6, 5631-5648, DOI 10.5194/acp-6-5631-2006, 2006.

1419 Spreitzer, E. J., Marschalik, M. P., and Spichtinger, P.: Subvisible cirrus clouds - a dynamical
1420 system approach, Nonlinear Proc Geoph, 24, 307-328, 10.5194/npg-24-307-2017, 2017.

1421 Tang, M. J., Cox, R. A., and Kalberer, M.: Compilation and evaluation of gas phase diffusion
1422 coefficients of reactive trace gases in the atmosphere: volume 1. Inorganic compounds, Atmos.
1423 Chem. Phys., 14, 9233-9247, 10.5194/acp-14-9233-2014, 2014.

1424 Thomas, A., Borrmann, S., Kiemle, C., Cairo, F., Volk, M., Beuermann, J., Lepuchov, B., Santacesaria,
1425 V., Matthey, R., Rudakov, V., Yushkov, V., MacKenzie, A. R., and Stefanutti, L.: In situ
1426 measurements of background aerosol and subvisible cirrus in the tropical tropopause region,
1427 Journal of Geophysical Research: Atmospheres, 107, AAC 8-1-AAC 8-14, 10.1029/2001jd001385,
1428 2002.

1429 Thomason, L. W., and Vernier, J. P.: Improved SAGE II cloud/aerosol categorization and
1430 observations of the Asian tropopause aerosol layer: 1989-2005, Atmos Chem Phys, 13, 4605-
1431 4616, 10.5194/acp-13-4605-2013, 2013.

1432 Tost, H., Lawrence, M. G., Brühl, C., Jöckel, P., The, G. T., and The, S.-O. D. A. T.: Uncertainties in
1433 atmospheric chemistry modelling due to convection parameterisations and subsequent
1434 scavenging, Atmos. Chem. Phys., 10, 1931-1951, 10.5194/acp-10-1931-2010, 2010.

1435 Tsagkogeorgas, G., Roldin, P., Duplissy, J., Rondo, L., Tröstl, J., Slowik, J. G., Ehrhart, S., Franchin,
1436 A., Kürten, A., Amorim, A., Bianchi, F., Kirkby, J., Petäjä, T., Baltensperger, U., Boy, M., Curtius, J.,
1437 Flagan, R. C., Kulmala, M., Donahue, N. M., and Stratmann, F.: Evaporation of sulfate aerosols at
1438 low relative humidity, Atmos. Chem. Phys., 17, 8923-8938, 10.5194/acp-17-8923-2017, 2017.

1439 Twohy, C. H., Clement, C. F., Gandrud, B. W., Weinheimer, A. J., Campos, T. L., Baumgardner, D.,
1440 Brune, W. H., Faloona, I., Sachse, G. W., Vay, S. A., and Tan, D.: Deep convection as a source of new
1441 particles in the midlatitude upper troposphere, J Geophys Res-Atmos, 107, Artn 4560

1442 10.1029/2001jd000323, 2002.

1443 Ueyama, R., Jensen, E. J., and Pfister, L.: Convective Influence on the Humidity and Clouds in the
1444 Tropical Tropopause Layer During Boreal Summer, J Geophys Res-Atmos, 123, 7576-7593,
1445 10.1029/2018jd028674, 2018.

1446 Ueyama, R., Jensen, E. J., Pfister, L., Krämer, M., Afchine, A., and Schoeberl, M.: Impact of
1447 Convectively Detrained Ice Crystals on the Humidity of the Tropical Tropopause Layer in Boreal
1448 Winter, Journal of Geophysical Research: Atmospheres, 125, e2020JD032894,
1449 10.1029/2020JD032894, 2020.

1450 Vehkamäki, H., Kulmala, M., Napari, I., Lehtinen, K. E. J., Timmreck, C., Noppel, M., and Laaksonen,
1451 A.: An improved parameterization for sulfuric acid–water nucleation rates for tropospheric and

https://doi.org/10.5194/acp-2020-1285
Preprint. Discussion started: 5 January 2021

1452 stratospheric conditions, Journal of Geophysical Research: Atmospheres, 107, AAC 3-1-AAC 3-
1453 10, 10.1029/2002jd002184, 2002.

1454 Venzac, H., Sellegri, K., Laj, P., Villani, P., Bonasoni, P., Marinoni, A., Cristofanelli, P., Calzolari, F.,
1455 Fuzzi, S., Decesari, S., Facchini, M. C., Vuillermoz, E., and Verza, G. P.: High frequency new particle
1456 formation in the Himalayas, P Natl Acad Sci USA, 105, 15666-15671, 10.1073/pnas.0801355105,
1457 2008.

1458 Vernier, J.-P., Fairlie, T. D., Deshler, T., Ratnam, M. V., Gadhavi, H., Kumar, B. S., Natarajan, M.,
1459 Pandit, A. K., Raj, S. T. A., Kumar, A. H., Jayaraman, A., Singh, A. K., Rastogi, N., Sinha, P. R., Kumar,
1460 S., Tiwari, S., Wegner, T., Baker, N., Vignelles, D., Stenchikov, G., Shevchenko, I., Smith, J., Bedka,
1461 K., Kesarkar, A., Singh, V., Bhate, J., Ravikiran, V., Rao, M. D., Ravindrababu, S., Patel, A., Vernier,
1462 H., Wienhold, F. G., Liu, H., Knepp, T. N., Thomason, L., Crawford, J., Ziemba, L., Moore, J.,
1463 Crumeyrolle, S., Williamson, M., Berthet, G., Jégou, F., and Renard, J.-B.: BATAL: The Balloon
1464 Measurement Campaigns of the Asian Tropopause Aerosol Layer, B Am Meteorol Soc, 99, 955-
1465 973, 10.1175/bams-d-17-0014.1, 2018.

1466 Vernier, J. P., Thomason, L. W., and Kar, J.: CALIPSO detection of an Asian tropopause aerosol
1467 layer, Geophys Res Lett, 38, Artn L07804

1468 10.1029/2010gl046614, 2011.

1469 Vernier, J. P., Fairlie, T. D., Natarajan, M., Wienhold, F. G., Bian, J., Martinsson, B. G., Crumeyrolle,
1470 S., Thomason, L. W., and Bedka, K. M.: Increase in upper tropospheric and lower stratospheric
1471 aerosol levels and its potential connection with Asian pollution, J Geophys Res-Atmos, 120,
1472 1608-1619, 10.1002/2014jd022372, 2015.

1473 Viciani, S., D'Amato, F., Mazzinghi, P., Castagnoli, F., Toci, G., and Werle, P.: A cryogenically
1474 operated laser diode spectrometer for airborne measurement of stratospheric trace gases,
1475 Applied Physics B, 90, 581-592, 10.1007/s00340-007-2885-2, 2008.

1476 Viciani, S., Montori, A., Chiarugi, A., and D'Amato, F.: A Portable Quantum Cascade Laser
1477 Spectrometer for Atmospheric Measurements of Carbon Monoxide, Sensors, 18, 2380,
1478 doi:10.3390/s18072380, 2018.

1479 Vogel, B., Günther, G., Müller, R., Grooss, J. U., Hoor, P., Krämer, M., Müller, S., Zahn, A., and Riese,
1480 M.: Fast transport from Southeast Asia boundary layer sources to northern Europe: rapid uplift
1481 in typhoons and eastward eddy shedding of the Asian monsoon anticyclone, Atmos Chem Phys,
1482 14, 12745-12762, 10.5194/acp-14-12745-2014, 2014.

1483 Vogel, B., Müller, R., Günther, G., Spang, R., Hanumanthu, S., Li, D., Riese, M., and Stiller, G. P.:
1484 Lagrangian simulations of the transport of young air masses to the top of the Asian monsoon
1485 anticyclone and into the tropical pipe, Atmos Chem Phys, 19, 6007-6034, 10.5194/acp-19-6007-
1486 2019, 2019.

1487 Waddicor, D. A., Vaughan, G., Choularton, T. W., Bower, K. N., Coe, H., Gallagher, M., Williams, P. I.,
1488 Flynn, M., Volz-Thomas, A., Patz, H. W., Isaac, P., Hacker, J., Arnold, F., Schlager, H., and Whiteway,
1489 J. A.: Aerosol observations and growth rates downwind of the anvil of a deep tropical
1490 thunderstorm, Atmos Chem Phys, 12, 6157-6172, 10.5194/acp-12-6157-2012, 2012.

1491 Wang, M., Kong, W., Marten, R., He, X.-C., Chen, D., Pfeifer, J., Heitto, A., Kontkanen, J., Dada, L.,
1492 Kürten, A., Yli-Juuti, T., Manninen, H. E., Amanatidis, S., Amorim, A., Baalbaki, R., Baccarini, A.,
1493 Bell, D. M., Bertozzi, B., Bräkling, S., Brilke, S., Murillo, L. C., Chiu, R., Chu, B., De Menezes, L.-P.,
1494 Duplissy, J., Finkenzeller, H., Carracedo, L. G., Granzin, M., Guida, R., Hansel, A., Hofbauer, V.,
1495 Krechmer, J., Lehtipalo, K., Lamkaddam, H., Lampimäki, M., Lee, C. P., Makhmutov, V., Marie, G.,

https://doi.org/10.5194/acp-2020-1285
Preprint. Discussion started: 5 January 2021

1496 Mathot, S., Mauldin, R. L., Mentler, B., Müller, T., Onnela, A., Partoll, E., Petäjä, T., Philippov, M.,
1497 Pospisilova, V., Ranjithkumar, A., Rissanen, M., Rörup, B., Scholz, W., Shen, J., Simon, M., Sipilä, M.,
1498 Steiner, G., Stolzenburg, D., Tham, Y. J., Tomé, A., Wagner, A. C., Wang, D. S., Wang, Y., Weber, S. K.,
1499 Winkler, P. M., Wlasits, P. J., Wu, Y., Xiao, M., Ye, Q., Zauner-Wieczorek, M., Zhou, X., Volkamer, R.,
1500 Riipinen, I., Dommen, J., Curtius, J., Baltensperger, U., Kulmala, M., Worsnop, D. R., Kirkby, J.,
1501 Seinfeld, J. H., El-Haddad, I., Flagan, R. C., and Donahue, N. M.: Rapid growth of new atmospheric
1502 particles by nitric acid and ammonia condensation, Nature, 581, 184-189, 10.1038/s41586-020-
1503 2270-4, 2020.

1504 Weber, R. J., Clarke, A. D., Litchy, M., Li, J., Kok, G., Schillawski, R. D., and McMurry, P. H.: Spurious
1505 aerosol measurements when sampling from aircraft in the vicinity of clouds, Journal of
1506 Geophysical Research: Atmospheres, 103, 28337-28346, 10.1029/98jd02086, 1998.

1507 Wehner, B., Werner, F., Ditas, F., Shaw, R. A., Kulmala, M., and Siebert, H.: Observations of new
1508 particle formation in enhanced UV irradiance zones near cumulus clouds, Atmos Chem Phys, 15,
1509 11701-11711, 10.5194/acp-15-11701-2015, 2015.

1510 Weigel, R., Hermann, M., Curtius, J., Voigt, C., Walter, S., Bottger, T., Lepukhov, B., Belyaev, G., and
1511 Borrmann, S.: Experimental characterization of the COndensation PArticle counting System for
1512 high altitude aircraft-borne application, Atmos Meas Tech, 2, 243-258, 10.5194/amt-2-243-
1513 2009, 2009.

1514 Weigel, R., Borrmann, S., Kazil, J., Minikin, A., Stohl, A., Wilson, J. C., Reeves, J. M., Kunkel, D., de
1515 Reus, M., Frey, W., Lovejoy, E. R., Volk, C. M., Viciani, S., D'Amato, F., Schiller, C., Peter, T., Schlager,
1516 H., Cairo, F., Law, K. S., Shur, G. N., Belyaev, G. V., and Curtius, J.: In situ observations of new
1517 particle formation in the tropical upper troposphere: the role of clouds and the nucleation
1518 mechanism, Atmos Chem Phys, 11, 9983-10010, 10.5194/acp-11-9983-2011, 2011.

1519 Weigel, R., Volk, C. M., Kandler, K., Hosen, E., Gunther, G., Vogel, B., Grooss, J. U., Khaykin, S.,
1520 Belyaev, G. V., and Borrmann, S.: Enhancements of the refractory submicron aerosol fraction in
1521 the Arctic polar vortex: feature or exception?, Atmos Chem Phys, 14, 12319-12342, DOI
1522 10.5194/acp-14-12319-2014, 2014.

1523 Weigel, R., Mahnke, C., Baumgartner, M., Dragoneas, A., Vogel, B., Ploeger, F., Viciani, S., D'Amato,
1524 F., Bucci, S., Legras, B., Luo, B., Belyaev, G. V., and Borrmann, S.: In-Situ observation of New
1525 Particle Formation in the upper troposphere / lower stratosphere of the Asian Monsoon
1526 Anticyclone, Atmos. Chem. Phys. Discuss., acp-2020-1158, 2020a.

1527 Weigelt, A., Hermann, M., van Velthoven, P. F. J., Brenninkmeijer, C. A. M., Schlaf, G., Zahn, A., and
1528 Wiedensohler, A.: Influence of clouds on aerosol particle number concentrations in the upper
1529 troposphere, J Geophys Res-Atmos, 114, Artn D01204

1530 10.1029/2008jd009805, 2009.

1531 Wernli, H., Boettcher, M., Joos, H., Miltenberger, A. K., and Spichtinger, P.: A trajectory-based
1532 classification of ERA-Interim ice clouds in the region of the North Atlantic storm track, Geophys
1533 Res Lett, 43, 6657-6664, 10.1002/2016gl068922, 2016.

1534 Williamson, C. J., Kupc, A., Axisa, D., Bilsback, K. R., Bui, T., Campuzano-Jost, P., Dollner, M., Froyd,
1535 K. D., Hodshire, A. L., Jimenez, J. L., Kodros, J. K., Luo, G., Murphy, D. M., Nault, B. A., Ray, E. A.,
1536 Weinzierl, B., Wilson, J. C., Yu, F., Yu, P., Pierce, J. R., and Brock, C. A.: A large source of cloud
1537 condensation nuclei from new particle formation in the tropics, Nature, 574, 399-403,
1538 10.1038/s41586-019-1638-9, 2019.

https://doi.org/10.5194/acp-2020-1285
Preprint. Discussion started: 5 January 2021

Atmospheric Chemistry and Physics Discussions

1539 Wilson, J. C., Stolzenburg, M. R., Clark, W. E., Loewenstein, M., Ferry, G. V., Chan, K. R., and Kelly, K.
1540 K.: Stratospheric Sulfate Aerosol in and near the Northern-Hemisphere Polar Vortex - the
1541 Morphology of the Sulfate Layer, Multimodal Size Distributions, and the Effect of Denitrification,
1542 J Geophys Res-Atmos, 97, 7997-8013, 10.1029/92JD00065, 1992.

1543 WMO: International Meteorological Tables, WMO-No.188.TP97, edited by: Letestu, S., Secretariat
1544 of the World Meteorological Organization, Geneva, Switzerland, 1966.

1545 Yin, Y., Chevallier, F., Ciais, P., Broquet, G., Fortems-Cheiney, A., Pison, I., and Saunois, M.: Decadal
1546 trends in global CO emissions as seen by MOPITT, Atmos. Chem. Phys., 15, 13433-13451,
1547 10.5194/acp-15-13433-2015, 2015.

1548 Yu, P. F., Toon, O. B., Neely, R. R., Martinsson, B. G., and Brenninkmeijer, C. A. M.: Composition and
1549 physical properties of the Asian Tropopause Aerosol Layer and the North American
1550 Tropospheric Aerosol Layer, Geophys Res Lett, 42, 2540-2546, 10.1002/2015gl063181, 2015.

1551 Zöger, M., Afchine, A., Eicke, N., Gerhards, M. T., Klein, E., McKenna, D. S., Morschel, U., Schmidt,
1552 U., Tan, V., Tuitjer, F., Woyke, T., and Schiller, C.: Fast in situ stratospheric hygrometers: A new
1553 family of balloon-borne and airborne Lyman alpha photofragment fluorescence hygrometers, J
1554 Geophys Res-Atmos, 104, 1807-1816, Doi 10.1029/1998jd100025, 1999.

1555

https://doi.org/10.5194/acp-2020-1285
Preprint. Discussion started: 5 January 2021

Atmospheric Chemistry and Physics Discussions

Figure captions

Figure 1: The flight patterns of the M-55 *Geophysica* during StratoClim 2017 over the Indian subcontinent. New particle formation (NPF) encountered in clear air along the flight tracks are indicated by orange colour in the main panel a). All NPF events coinciding with the detection of cloud (ice) particles are coloured in blue. The general perspective, b), exhibits the patterns of the eight StratoClim flights over Nepal, North - East India, Bangladesh, and the Bay of Bengal. For more details, see Table 1.

Figure 2: The 1-Hz resolved number concentrations of aerosol particles in the ultrafine size range (N_{uf}) and of cloud (ice) particles (N_{ice}) of the eight StratoClim flights compiled in one time series ranging from 03:30 (UTC) to 12:30 (UTC). Kathmandu's (Nepal) local noontime is indicated by the vertical orange line (corresponding to 06:15 UTC, or 22500 seconds of day, UTC). Data points of N_{uf} in black whenever N_{ice} (cyan) equals zero, otherwise N_{uf} is coloured in red. The blue dashed line indicates the median N_{ice} (0.031 cm^{-3}) for the entire dataset of cloud particle detections during StratoClim 2017 (Krämer et al., 2020).

Figure 3: Vertical profiles of the mixing ratio (1-Hz resolved) of aerosols in the ultrafine size range (n_{uf}) versus the potential temperature (θ). a): all data separated concerning coincident detection of cloud (ice) particles (black: $N_{ice} = 0$ cm^{-3}, red: $N_{ice} > 0$ cm^{-3}) and b): all data coloured correspondingly to the flight date, c): exclusively for $N_{ice} > 0$ cm^{-3}; d): when $N_{ice} = 0$ cm^{-3}. In the panels at the bottom (e and f) in-cloud and clear-air measurements are distinguished correspondingly to the intermediate panels (c and d) and coloured with reference to carbon monoxide (CO) mixing ratios.

Figure 4: Histograms of the occurrence frequency of number concentrations N_{uf} of all NPF detections (1-Hz resolved) throughout StratoClim 2017. a): all data of N_{uf} in general (black) and separated concerning coincident detection of cloud (ice) particles in the diameter size range 3 µm < d_p < 937 µm (green: $N_{ice} = N_{3\text{-}937\mu m} = 0$ cm^{-3}, red: $N_{ice} > 0$ cm^{-3}). Hence, the sum of the green and red curve yield the black curve, the vertical bars of which represent the square route of count values. b): relative occurrence frequency of N_{uf} for in-cloud NPF (if detected coincidently with $N_{ice} > 0$ cm^{-3}) normalised with respect to all NPF detections, i.e. the ratio of the absolute occurrence frequencies (in red and black, Panel a). c): relative occurrence frequency of N_{uf} for in-cloud NPF, if detected coincidently with various N_{ice} levels, which were normalised with respect to those NPF detections with $N_{ice} > 0$ cm^{-3}, (in red, Panel b).

Figure 5: The total aerosol number concentration versus cloud particle number concentration in accordance to de Reus et al. (2009). The total number concentration N_{10} measured with one of four COPAS channels together with coincident detections of N_{ice} (i.e. $N_{3\text{-}937\mu m}$) by the NIXE-CAPS. The data points are averaged over at least 10 s of flight time, and the bars exhibit the standard deviation over the averaging periods. The data points are colour-coded in a) with reference to *IWC*. b): NPF encounters (orange) throughout the averaging period (otherwise: grey). The blue-shaded areas in both panels indicate the range of most of the data points provided by de Reus et al. (2009).

Figure 6: NPF in the *IWC* - *T* parameter space (cf. Krämer et al. (2016)): measured ice water content (*IWC*) coincidently detected with COPAS data as a function of ambient air temperature throughout StratoClim 2017 (1-Hz resolved) – data points are colour-coded referring to (a) the

https://doi.org/10.5194/acp-2020-1285
Preprint. Discussion started: 5 January 2021

Atmospheric Chemistry and Physics Discussions

detected mixing ratios of ultrafine particles, n_{uf}, (b) the total mixing ratio n_6 measured with one of four COPAS channels and (c) the carbon monoxide (CO) mixing ratio. Note: in (a), the data points are grey if data of $n_{6\text{-}15}$ are available, while colours are apportioned only to those n_{uf} (i.e. $n_{6\text{-}15}$) complying with the NPF criterion. Generally, the black lines represent the median (solid) and the upper-/lowermost bounds (dashed) of the core *IWC* band, respectively, as obtained from earlier measurements at other locations (Krämer et al. (2016)).

Figure 7: The 1-Hz resolved concentration of in-cloud detected ultrafine aerosol (N_{uf}) as a function of the mean inter-crystal distance, *ICD*, between encountered cloud (ice) particles colour-coded with reference to (a) the number concentration of cloud ice particles, (b) to *IWC*, and (c) to the mean ice particles' radius.

Figure 8: The 1-Hz resolved concentration of ultrafine aerosol (N_{uf}) as a function of the cloud (ice) particles' integral radius, $IR = \overline{r_{ice}} \cdot N_{ice}$ (with $\overline{r_{ice}}$, ice particles' mean mass radius) colour-coded in correspondence to detected ice water content (*IWC*, panel a) and to measured CO mixing ratio (b); in the absence of CO values the data points are blackened. The diagonal, grey-coloured bars indicate a break-off edge along which the NPF seems limited by the *IR* in general, with two exceptional encounters of very recent or just proceeding NPF (see text for details).

Figure B- 1: Simulated change of the H_2SO_4 vapour's saturation ratio as a function of time due to the presence of entirely H_2SO_4 - coated ice particle surfaces of various sizes and number concentrations. a): particles with radii r_p = 1 µm, b): r_p = 10 µm; c): r_p = 100 µm. Overall, this simulation covers a range of integral radii *IR* (= $\overline{r_{ice}} \cdot N_{ice}$) from 0.01 to 10 µm cm^{-3}. Note: a cloud (ice) particle is assumed as coated with H_2SO_4 (consistent with Bogdan et al. (2006); Bogdan et al. (2013)).

https://doi.org/10.5194/acp-2020-1285
Preprint. Discussion started: 5 January 2021

Atmospheric Chemistry and Physics Discussions

Figures

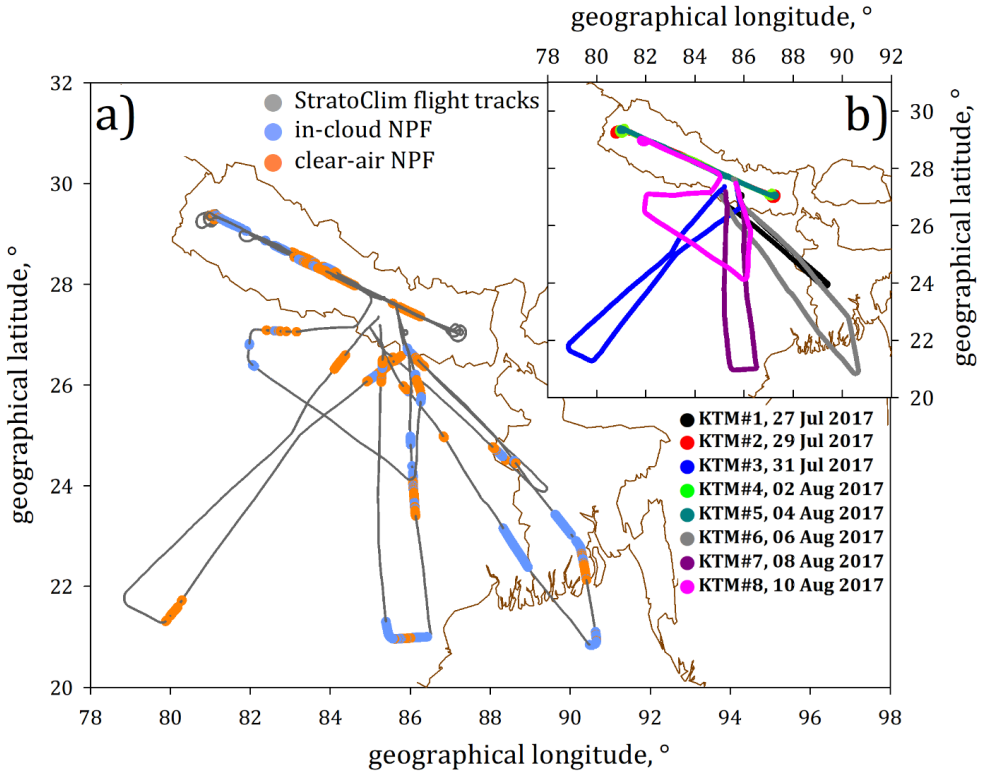

Figure 1

https://doi.org/10.5194/acp-2020-1285
Preprint. Discussion started: 5 January 2021

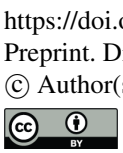

Atmospheric Chemistry and Physics Discussions

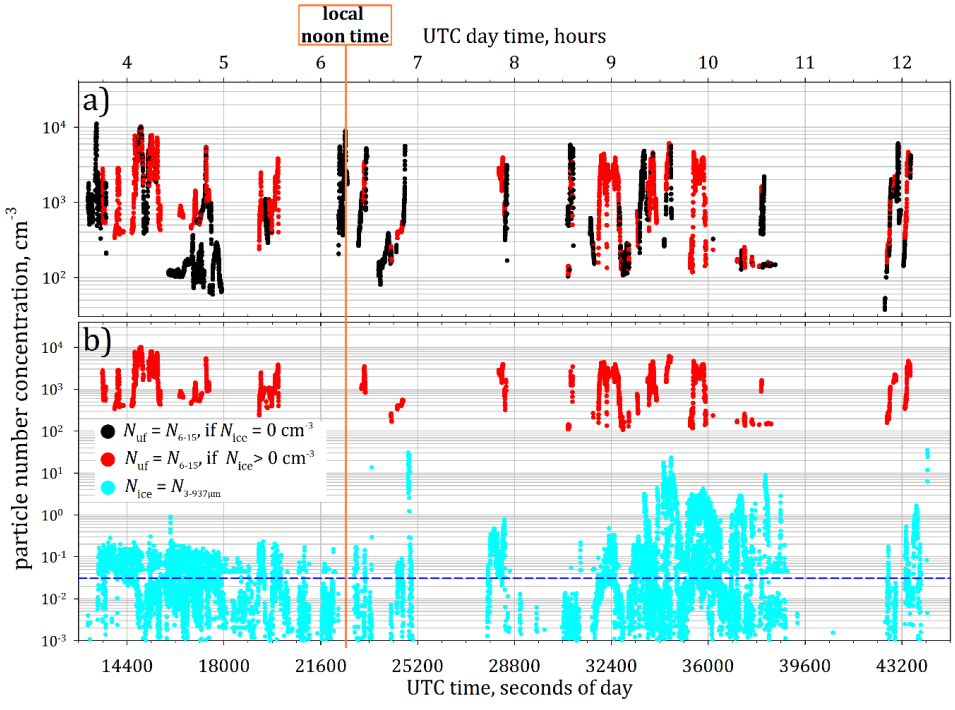

Figure 2

https://doi.org/10.5194/acp-2020-1285
Preprint. Discussion started: 5 January 2021

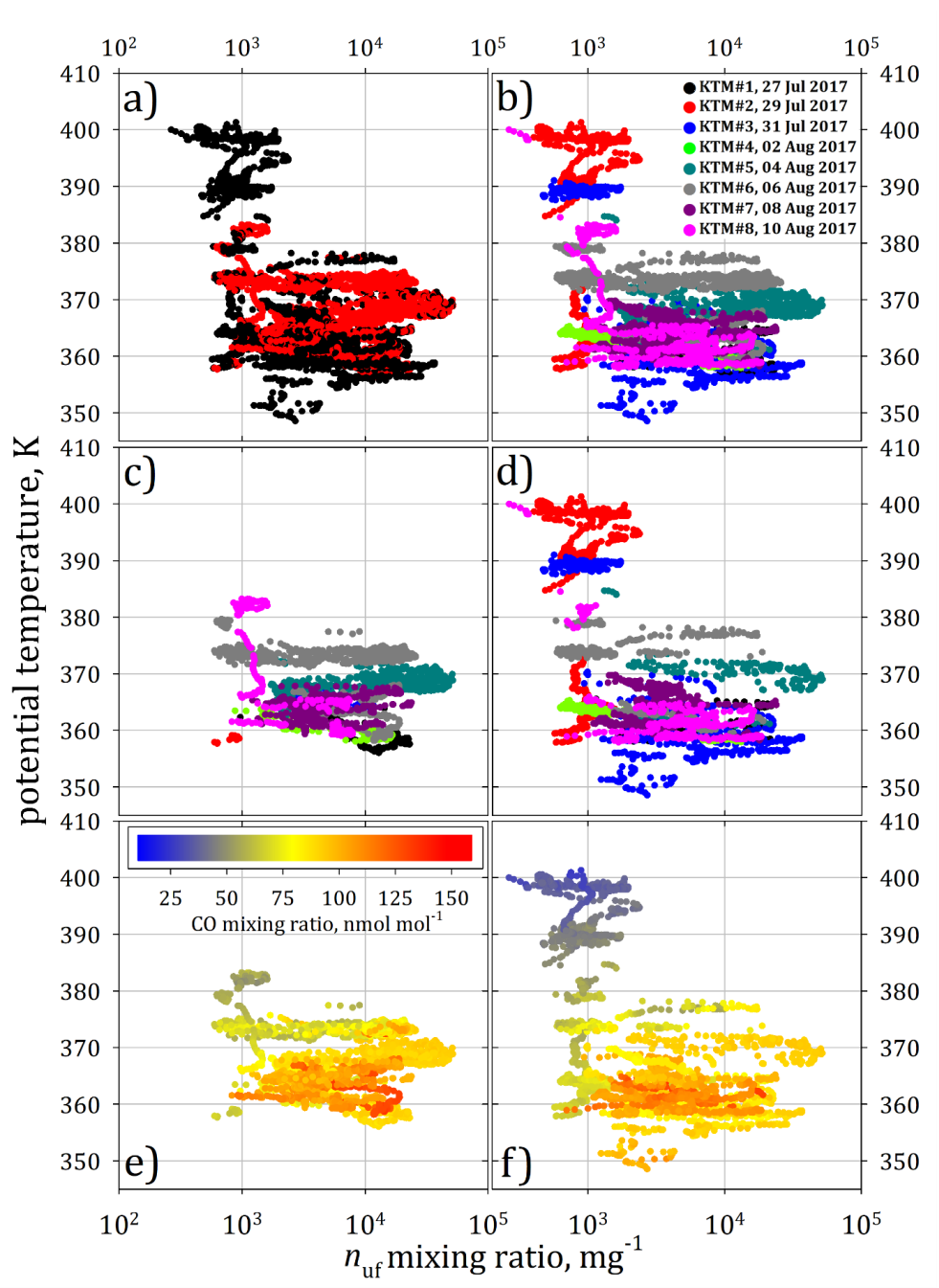

Figure 3

https://doi.org/10.5194/acp-2020-1285
Preprint. Discussion started: 5 January 2021

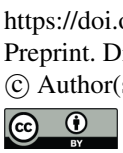

Atmospheric Chemistry and Physics Discussions

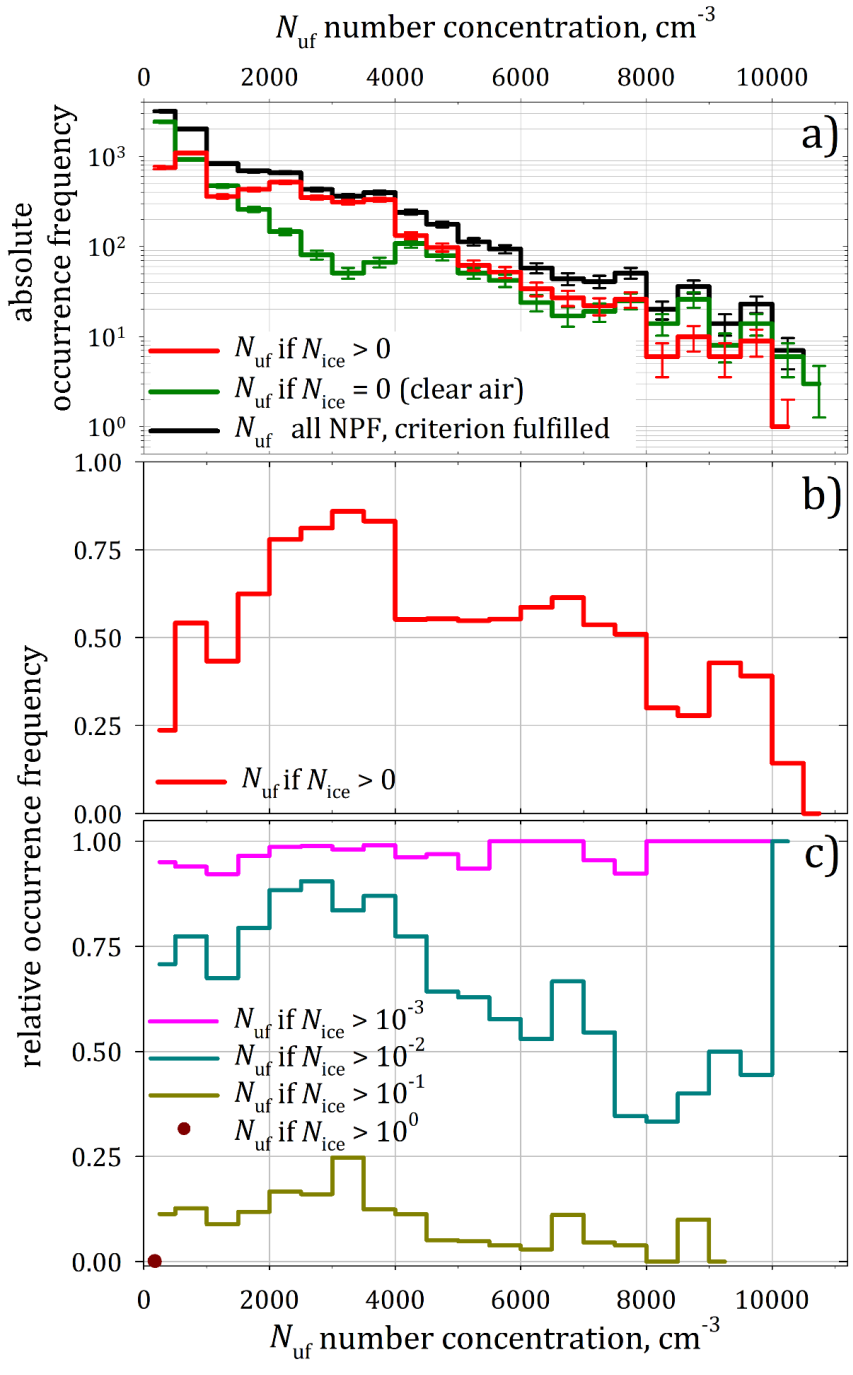

Figure 4

https://doi.org/10.5194/acp-2020-1285
Preprint. Discussion started: 5 January 2021

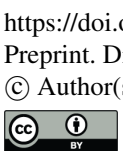

Atmospheric Chemistry and Physics Discussions

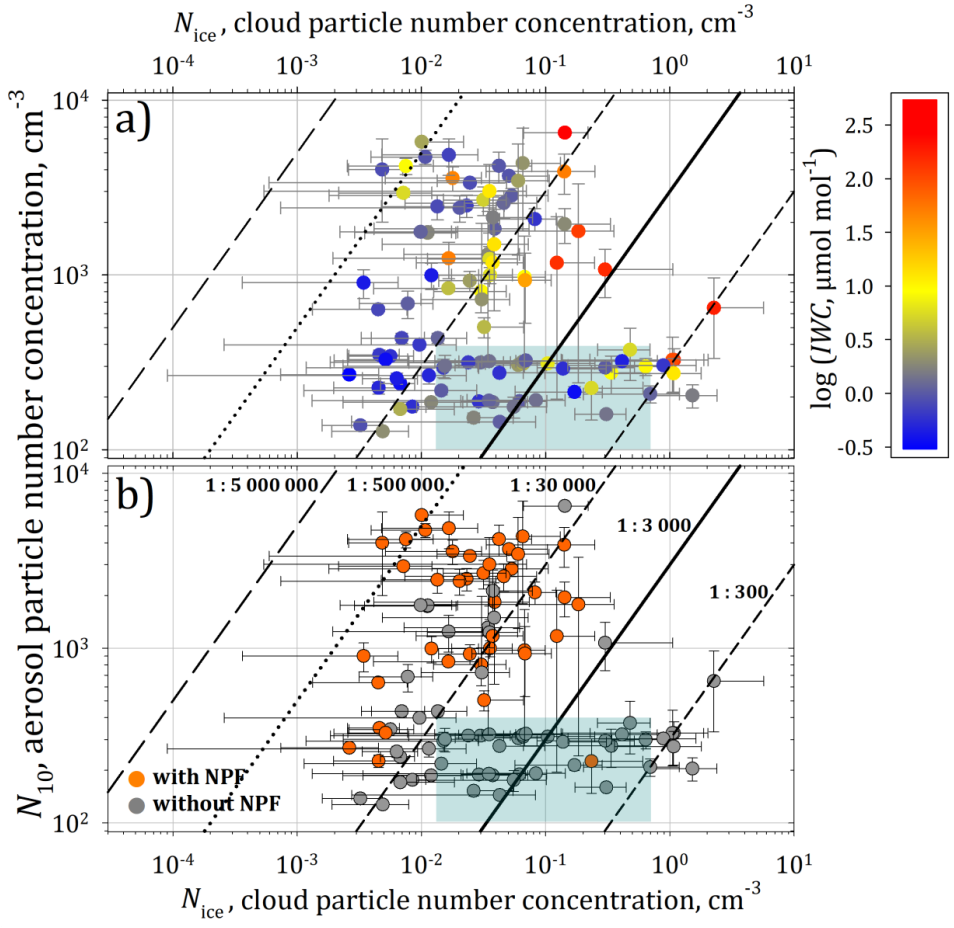

Figure 5

https://doi.org/10.5194/acp-2020-1285
Preprint. Discussion started: 5 January 2021

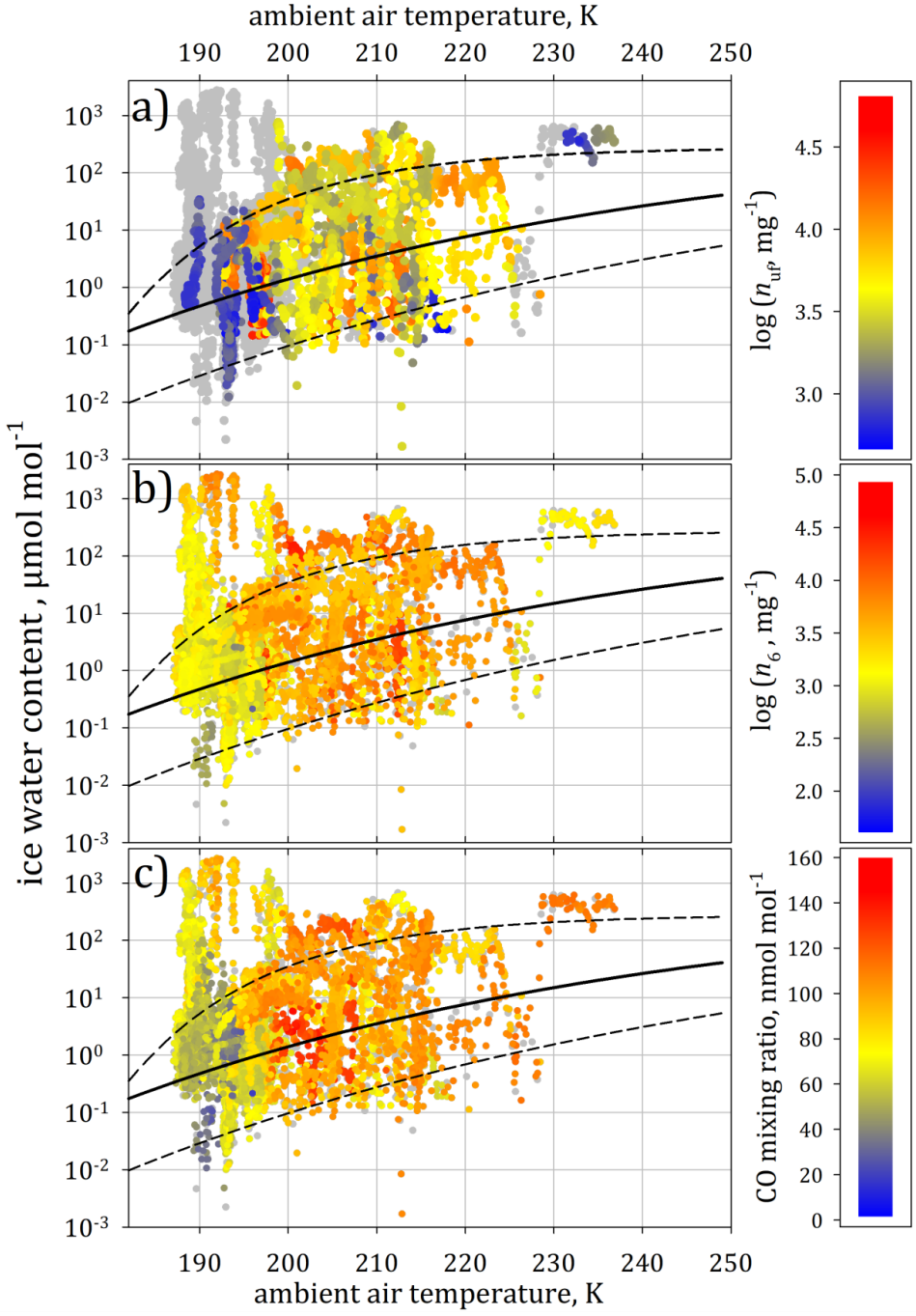

Figure 6

https://doi.org/10.5194/acp-2020-1285
Preprint. Discussion started: 5 January 2021

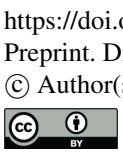

Atmospheric Chemistry and Physics Discussions

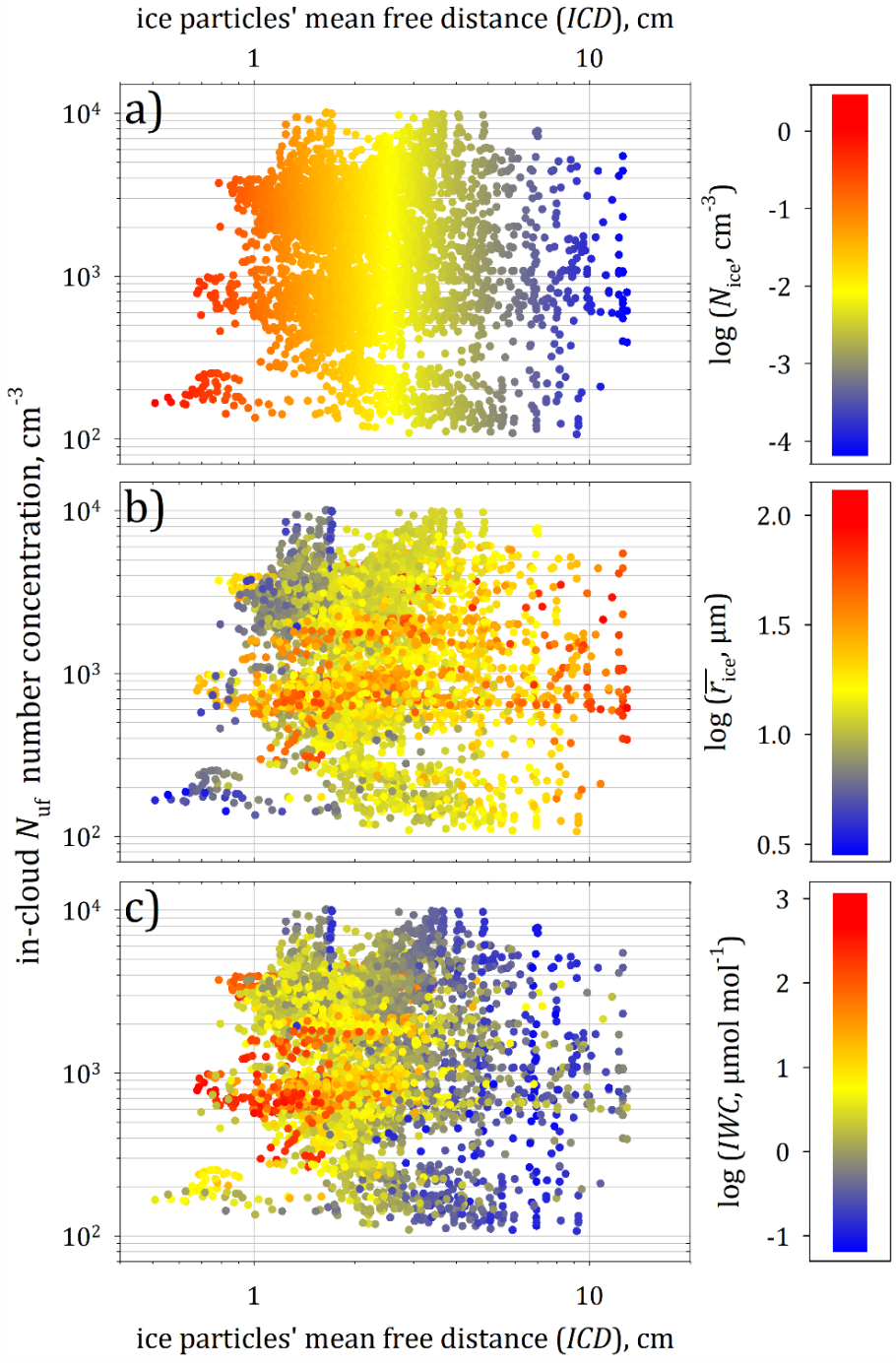

Figure 7

https://doi.org/10.5194/acp-2020-1285
Preprint. Discussion started: 5 January 2021

Atmospheric Chemistry and Physics Discussions

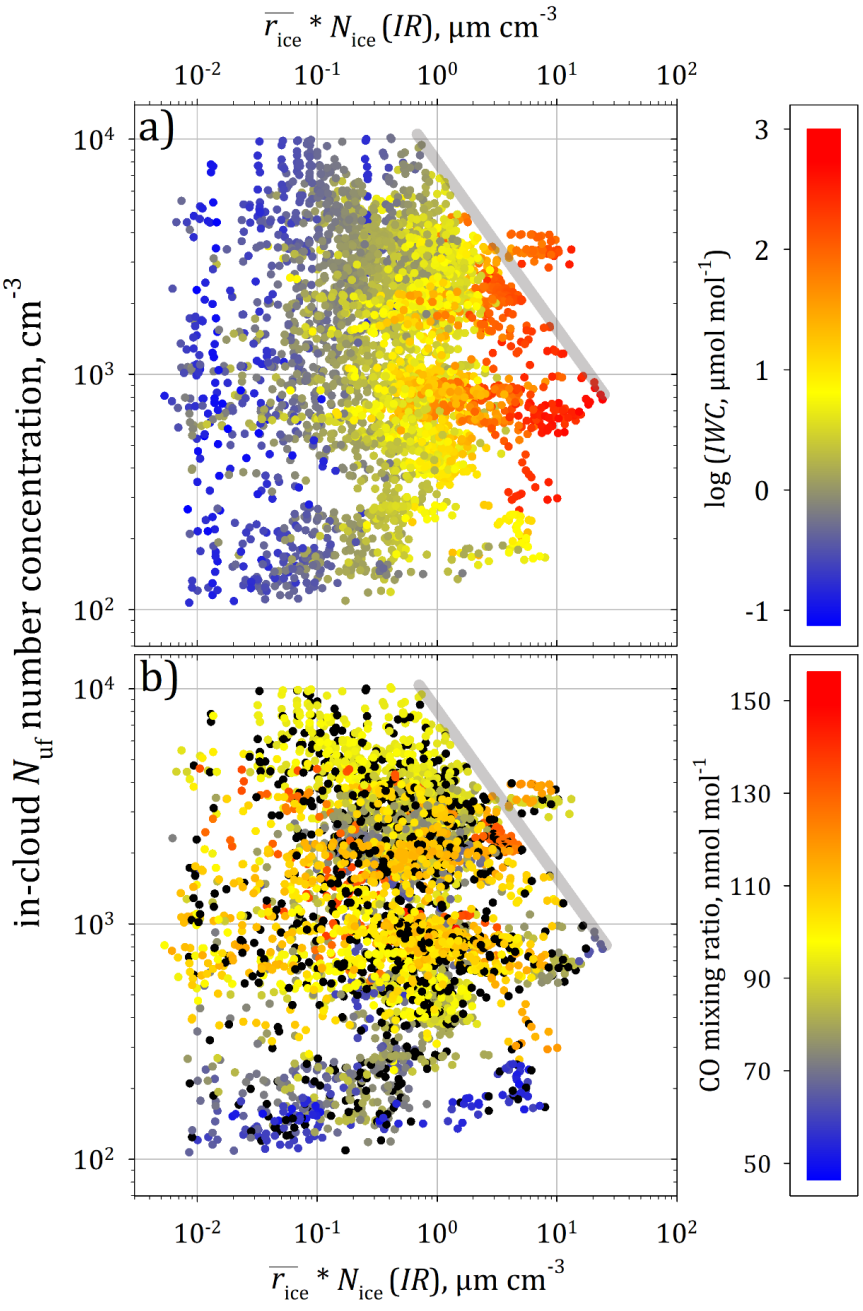

Figure 8

https://doi.org/10.5194/acp-2020-1285
Preprint. Discussion started: 5 January 2021

Atmospheric Chemistry and Physics Discussions

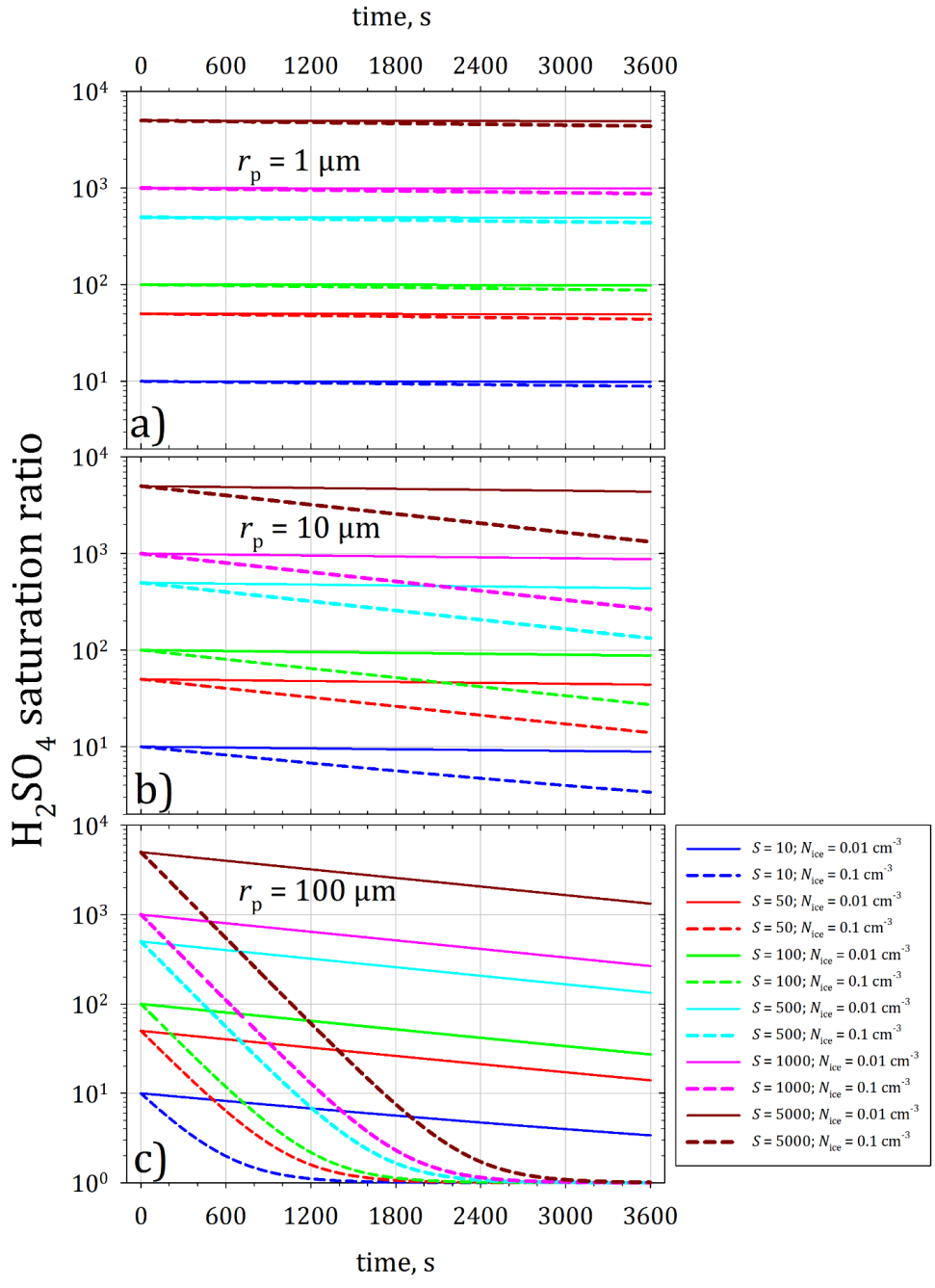

Figure B- 1

https://doi.org/10.5194/acp-2020-1285
Preprint. Discussion started: 5 January 2021

Atmospheric Chemistry and Physics Discussions

Table 1: NPF data set of StratoClim 2017, separated by event detection under clear-air (i.e. N_{ice} = 0 cm^{-3}) and in-cloud conditions (i.e. N_{ice} > 0 cm^{-3}). Discussed in-cloud NPF events (104 incidents that comply with introduced NPF criterion, Section 2.2) are partially embedded in larger clear-air NPF fields with continuously elevated N_{uf}. The total number of measurement seconds with NPF detections under either of both conditions is scaled to the total data set of the CN measurements and the total duration of NPF encounters. The mean horizontal distance is calculated from the event duration based on a mean flight speed of the M-55 *Geophysica* (154 ± 39 m s^{-1}, variable flight attitude remains unconsidered) and may be understood as equivalent horizontal extension of a NPF event. The total measurement time of in-cloud NPF encounters is categorised into vertically stacked bins of 5 K potential temperature.

	total duration		percentage of		mean horizontal
NPF condition	seconds	hh : mm	NPF data	total dataset	distance in km
clear-air	4866	01 : 21	~ 51.2 %	~ 5.3 %	~ 750
in-cloud	4634	01 : 17	~ 48.8 %	~ 5.0 %	~ 714

			in-cloud NPF	
potential	total duration		percentage of	mean horizontal
temperature	seconds	hh : mm	in-cloud NPF	distance in km
355 – 360 K	432	00 : 07	~ 9.3 %	~ 67
360 – 365 K	1231	00 : 21	~ 26.6 %	~ 190
365 – 370 K	1455	00 : 24	~ 31.4 %	~ 224
370 – 375 K	1375	00 : 23	~ 29.7 %	~ 212
> 375 K	141	00 : 02	~ 3 %	~ 22